# Growth of the Qaidam Basin during Cenozoic exhumation in the northern Tibetan Plateau: Inferences from depositional patterns and multiproxy detrital provenance signatures

**Meredith A. Bush[1], Joel E. Saylor[2], Brian K. Horton[3], and Junsheng Nie[4]**

[1]DEPARTMENT OF GEOLOGICAL SCIENCES, JACKSON SCHOOL OF GEOSCIENCES, UNIVERSITY OF TEXAS AT AUSTIN, AUSTIN, TEXAS 78712, USA
[2]DEPARTMENT OF EARTH AND ATMOSPHERIC SCIENCES, UNIVERSITY OF HOUSTON, HOUSTON, TEXAS 77204-5007, USA
[3]DEPARTMENT OF GEOLOGICAL SCIENCES AND INSTITUTE FOR GEOPHYSICS, JACKSON SCHOOL OF GEOSCIENCES, UNIVERSITY OF TEXAS AT AUSTIN, AUSTIN, TEXAS 78712, USA
[4]MOE KEY LABORATORY OF WESTERN CHINA'S ENVIRONMENTAL SYSTEMS, COLLEGE OF EARTH AND ENVIRONMENTAL SCIENCES, LANZHOU UNIVERSITY, LANZHOU 73000, CHINA

## ABSTRACT

Sedimentologic and provenance analyses for the Qaidam Basin in the northern Tibetan Plateau help to elucidate the stratigraphic signatures of initial deformation and exhumation in basin-bounding ranges. The basin recorded sedimentary transitions in response to uplift and unroofing of several distinctive source regions. Along the NE basin margin, a detrital record of exhumation and basin isolation is preserved in the 6200-m-thick Cenozoic succession at the Dahonggou anticline. An up-section shift from axial fluvial and marginal lacustrine deposition to transverse fluvial sedimentation suggests progradation and increasingly proximal sediment sources, reflecting activation and advance of crustal deformation. Provenance results from sandstone petrology, U-Pb geochronology, and heavy mineral analyses indicate initial late Paleocene–early Eocene derivation from igneous, metamorphic, and sedimentary sources, consistent with Permian–Triassic arc rocks dominating the southern (Kunlun Shan) or southwestern (Qimen Tagh) basin margins. Up-section variations in sediment composition and detrital zircon U-Pb age distributions are attributed to Eocene–Oligocene derivation from lower Paleozoic and Mesozoic igneous and metamorphic rocks of the central to northern Qilian Shan–Nan Shan. Disappearance of igneous sources and persistence of metamorphic sources are consistent with derivation from the southern Qilian Shan–Nan Shan during early–middle Miocene shortening along the frontal Nan Shan–North Qaidam thrust belt. These results are supported by paleocurrent analyses revealing an Eocene shift from roughly E-directed (axial) to SW-directed (transverse) dispersal of sediment. Variations in lithofacies, composition, U-Pb ages, and paleoflow are consistent with late Paleocene–early Eocene exhumation in the Kunlun Shan followed by middle Eocene–middle Miocene exhumation in the Qilian Shan–Nan Shan. The up-section disappearance and reappearance of diagnostic U-Pb age populations can be associated with progressive unroofing of multiple thrust sheets, successive input of sedimentary and magmatic sources, and southward encroachment of Qilian Shan–Nan Shan shortening into the Qaidam Basin. The sedimentary record presented here indicates that during the Paleogene, the unified Qaidam-Tarim Basin was partitioned and uplifted as it was incorporated into the growing Tibetan Plateau. Comparison with basins on and surrounding the Tibetan Plateau suggests that basement strength and lateral homogeneity, and formation of syndepositional structural dams are among the primary controls on formation of giant sedimentary basins.

LITHOSPHERE; v. 8; no. 1; p. 58–82; GSA Data Repository Item 2015362 | Published online 7 December 2015 doi:10.1130/L449.1

## INTRODUCTION

The 5–14-km-thick Cenozoic succession in the Qaidam Basin (Fig. 1) provides an important detrital record of the intraplate response to the India-Asia collision. Growth of this internally drained basin at ~2500 m elevation has been ascribed to northward advance of Neogene collisional deformation and accompanying flexural subsidence (Meyer et al., 1998; Métivier et al., 1998; Tapponnier et al., 2001). However, evidence for pre-Neogene shortening in the northern Tibetan Plateau contradicts the proposed systematic northward propagation of deformation. Specifically, rapid late Eocene–Oligocene sedimentation and tectonic rotation (Horton et al., 2004; Dupont-Nivet et al., 2004, 2008), exhumational cooling (Clark et al., 2010), and thrust faulting (Duvall et al., 2011) indicate early deformation in northeastern Tibet (see review by Yuan et al., 2013). These findings highlight the limited understanding of early Cenozoic deformation and plate-interior basin evolution within the Tibetan Plateau.

Contrasting reconstructions have been proposed for mountain ranges bounding the Qaidam Basin. To the south, the eastern Kunlun Shan records pre-Cenozoic deformation (Cheng et al., 2015), an early phase of Eocene shortening (Jolivet et al., 2003; Yin et al., 2007a; Duvall et al., 2013), and complex Oligocene to Quaternary transpressional deformation ranging from ca. 30–20 Ma in the central range (Mock et al., 1999; Wang et al., 2004; Yuan et al., 2006; Clark et al., 2010; Mao et al., 2014) to 12–8 Ma in the west and 8–5 Ma in the east (Duvall et al., 2013). Left-lateral slip on the Kunlun fault initiated by middle–late Miocene time (Kirby et al., 2007; Fu and Awata, 2007; Duvall et al., 2013). To the north, the Qilian Shan–Nan Shan may record early Cenozoic faulting and middle–late Cenozoic migration of deformation and sedimentation to the south and east (Yin et al., 2008a). In contrast, thermochronology studies in the northern Qilian Shan identify bedrock cooling at 12–6 Ma (Zheng et al., 2010; Craddock et al., 2011b).

Continuous sediment accumulation in the Qaidam Basin from the Paleogene to Holocene may

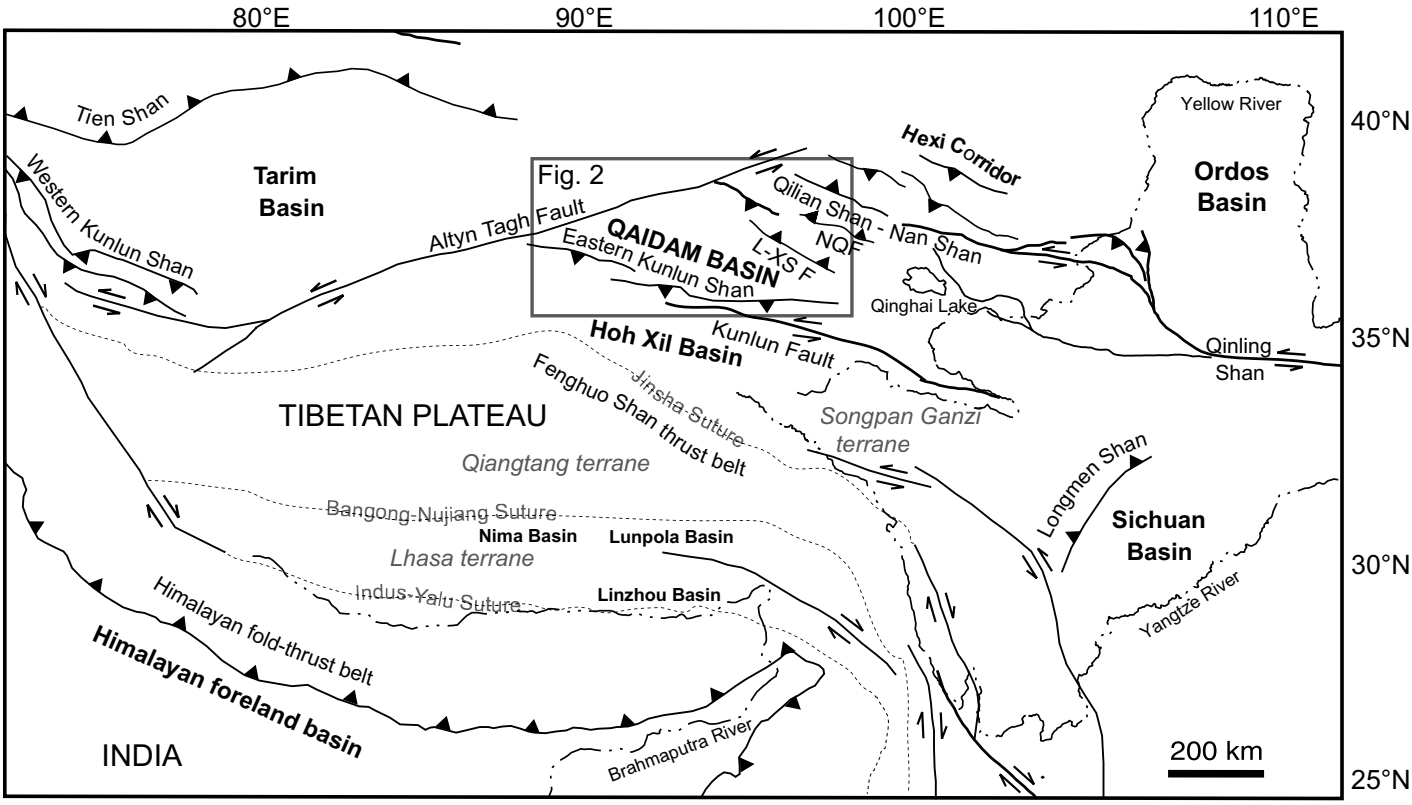


**Figure 1. Tectonic map of the Tibetan Plateau and adjacent regions showing major faults, Cenozoic basins, terranes, sutures, and rivers (adapted from Horton et al., 2004). L-XS F—Luliang Shan–Xitie Shan fault; NQF—North Qaidam fault.**

record the onset of exhumation in basin-bounding ranges, and associated changes in sediment sources. However, the Qaidam Basin epitomizes the challenge posed by plate-interior basins, in which multiple sediment sources are characterized by similar lithologies, compositions, or thermal histories (e.g., Graham et al., 1993). Sediment provenance tracers are often consistent with multiple potential sources and do not point to systematic up-section changes in sediment sourcing (Rieser et al., 2005, 2006a, 2006b; Zhuang et al., 2011; Jian et al., 2013; Cheng et al., 2015). However, application of multiple provenance techniques has identified changes in sediment sources (e.g., Hanson, 1999).

This study addresses the evolution of the Qaidam Basin by integrating multiple sedimentologic and provenance records from the northeastern margin of the basin to evaluate Cenozoic exhumation patterns in major basin-bounding ranges. Uniting stratigraphic and sedimentologic relationships with multiple provenance techniques, including petrographic, U-Pb geochronologic, heavy mineral, and paleocurrent analyses, sheds light on the growth of flanking ranges and associated evolution of Qaidam depositional systems. Interpretations of detrital zircon U-Pb results are guided by multidimensional scaling, a visualization technique representing statistical similarity among samples. Collectively, these data sets identify the early intraplate response to India-Asia collision through identification of nonuniform exhumation along Qaidam Basin margins.

## GEOLOGIC SETTING

The Qaidam Basin is surrounded by diverse igneous and metamorphic rocks constituting Precambrian basement, Paleozoic–Mesozoic magmatic arc, and accretionary prism assemblages overlapped by Mesozoic–Cenozoic basin fill. Flanking ranges (Figs. 1 and 2) include the Qilian Shan–Nan Shan system to the north, Kunlun Shan to the south, Altyn Shan to the west, and Ela Shan and Dulan-Chaka highland to the east.

The basin is commonly modeled as a rigid block composed of strong lithosphere and continental basement (Clark and Royden, 2000; Braitenberg et al., 2003; Dayem et al., 2009). Crystalline basement in northern Tibet is composed of the Qilian and Qaidam terranes: Proterozoic and Paleozoic assemblages accreted to the Tarim and Sino-Korean cratons during Paleozoic–early Mesozoic closure of the Tethys Ocean (Hsü et al., 1995; Sobel and Arnaud, 1999; Yin and Harrison, 2000; Yin et al., 2007b; Pullen et al., 2008; Gehrels et al., 2011).

To the north-northeast, the Qilian Shan–Nan Shan (Figs. 1 and 2) forms a major NW-trending fold-thrust belt overprinting a system originally formed during early Paleozoic collision and arc accretion and later reactivated during Mesozoic–Cenozoic extension, contraction, and strike-slip deformation (Ritts and Biffi, 2001; Jolivet et al., 2001; Xiao et al., 2009; Yan et al., 2010; Zheng et al., 2010). Synorogenic deposits in the adjacent Hexi Corridor document the onset of crustal shortening in the northern Qilian Shan by the Miocene (Wang and Coward, 1990; George et al., 2001; Bovet et al., 2009).

To the south, the E-trending Eastern Kunlun Shan (Figs. 1 and 2) is a transpressional fold-thrust system overprinting a Permian–Triassic magmatic arc (Dewey et al., 1988; Mock et al., 1999; Jolivet et al., 2001, 2003; Xiao et al., 2002; Mo et al., 2007; Yuan et al., 2009; Clark et al., 2010) and early Paleozoic arc in the westernmost Qimen Tagh range (W. Li et al., 2013). Left-lateral displacement along the Kunlun fault is thought to have initiated with late Miocene extension in southern Tibet and continues to the present (Van der Woerd et

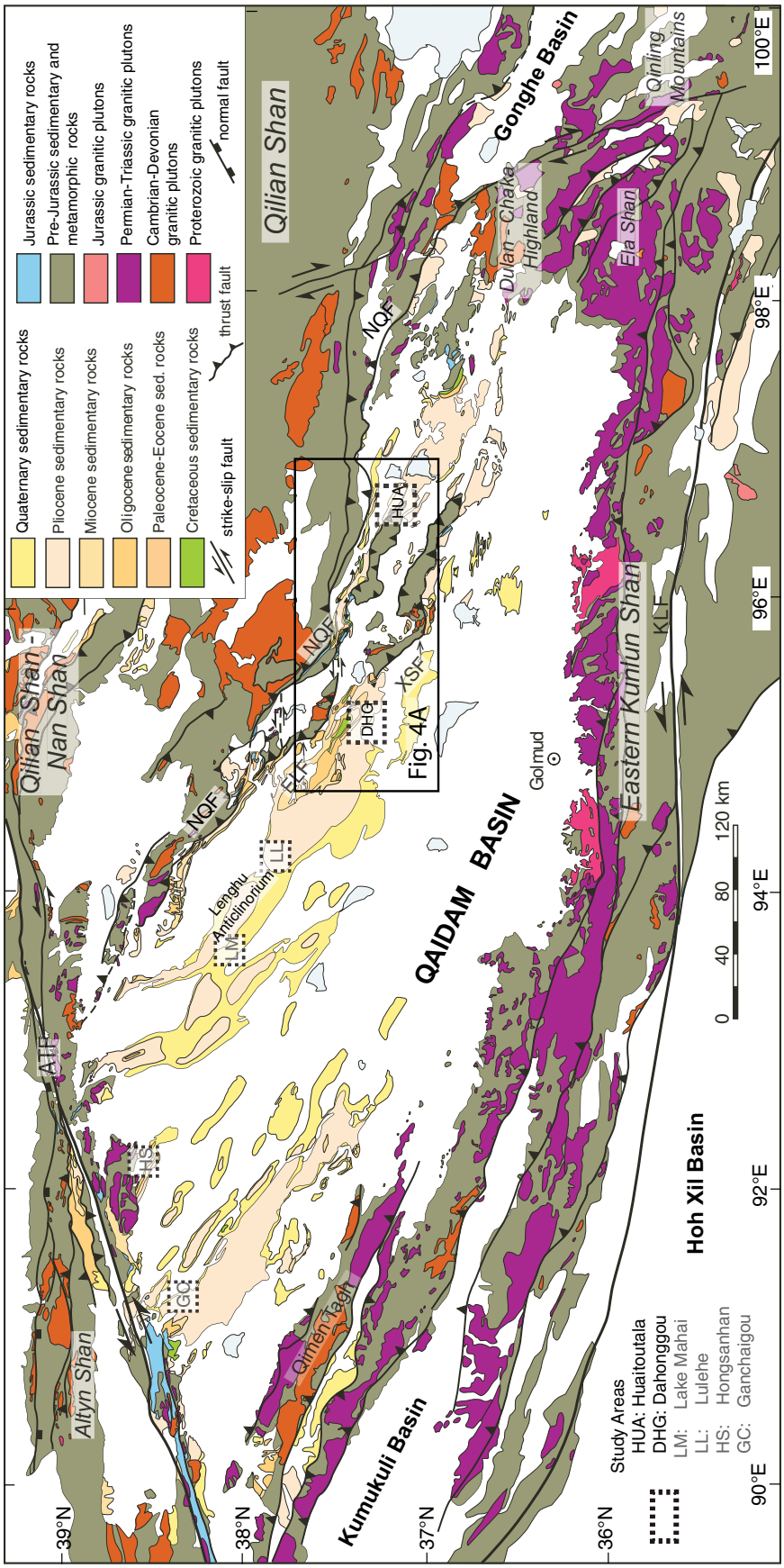


**Figure 2. Geologic map of the Qaidam Basin (modified from Chen et al., 2012) and surrounding areas showing major structures, rock units, and study localities (dashed boxes) DHG and HUA (this study) and LM, LL, GC, and HS (Zhuang et al., 2011). ATF—Altyn Tagh fault; ELF—East Luliang fault; KLF—Kunlun fault; NQF—North Qaidam fault; XSF—Xitie Shan thrust.**

al., 1998; Lin et al., 2002; Fu and Awata, 2007; Kirby et al., 2007; Duvall et al., 2013).

To the northwest, the NE-striking Altyn Tagh fault (Figs. 1 and 2) persists for 1600 km, with left-lateral displacement absorbed by NE-SW shortening in the Qilian Shan–Nan Shan. Altyn Tagh deformation initiated between 49 and 30 Ma, with strike-slip motion dominant by Miocene time, and progressively decreasing strike-slip motion (Jolivet et al., 2001; Yin et al., 2002; Wang et al., 2005) related to a shift from plate-like lateral extrusion to distributed crustal shortening (Yue et al., 2004; Ritts et al., 2008; Yin et al., 2008a, 2008b).

To the east, the Qaidam Basin is flanked by the Ela Shan range and Dulan-Chaka highland (Fig. 2), which form the boundary between Qaidam and externally drained Neogene basins of northeastern Tibet. These include the Miocene–Pliocene Gonghe, Xunhua, and Chaka basins, which occupy the Yellow River headwaters (Craddock et al., 2011b; Lease et al., 2011; Lu et al., 2012; H.-P. Zhang et al., 2012).

Ages of the Paleocene–Quaternary succession in the Qaidam Basin, based on nonmarine fossil assemblages and magnetostratigraphy (Fig. 3), have been extrapolated across the basin on the basis of seismic reflectors (QBGMR, 1991; Yang et al., 1992; Sun et al., 2005; Rieser et al., 2005, 2006a; Zhang, 2006; Fang et al., 2007; Wang et al., 2007; Gao et al., 2009; Lu and Xiong, 2009). However, ages from critical sedimentary sections are often only broadly constrained due to a lack of key marker beds. This study presents sedimentologic and multiproxy provenance results for the northern basin margin (Figs. 2 and 4), complementing magnetostratigraphic, paleoclimatologic, and paleontological data from the Dahonggou and Huaitoutala anticlines (Fang et al., 2007; Wang et al., 2007; Lu and Xiong, 2009; Zhuang et al., 2011; Song et al., 2013a, 2013b). Ages used here are consistent with the regional study conducted by Zhuang et al. (2011) and published magnetostratigraphic results from the two sections examined here (Fang et al., 2007; Lu and Xiong, 2009). A 6200-m-thick stratigraphic section was measured on the southern limb of the Dahonggou anticline west of Xitieshanzhen (37.5486°N, 95.1655°E). Continuous exposures include the upper Paleocene–Eocene Lulehe (~1100 m), Eocene Xiaganchaigou (~2400 m), Oligocene Shangganchaigou (~1300 m), lower Miocene Xiayoushashan (~800 m), middle–upper Miocene Shangyoushashan (~300 m), upper Miocene–Pliocene Shizigou (300 m), and overlapping Quaternary Qigequan Formations (Fig. 3). Although the lower 3500 m section of the Cenozoic succession remains poorly dated, magnetostratigraphic and sedimentologic studies of neighboring sections have constrained the age of

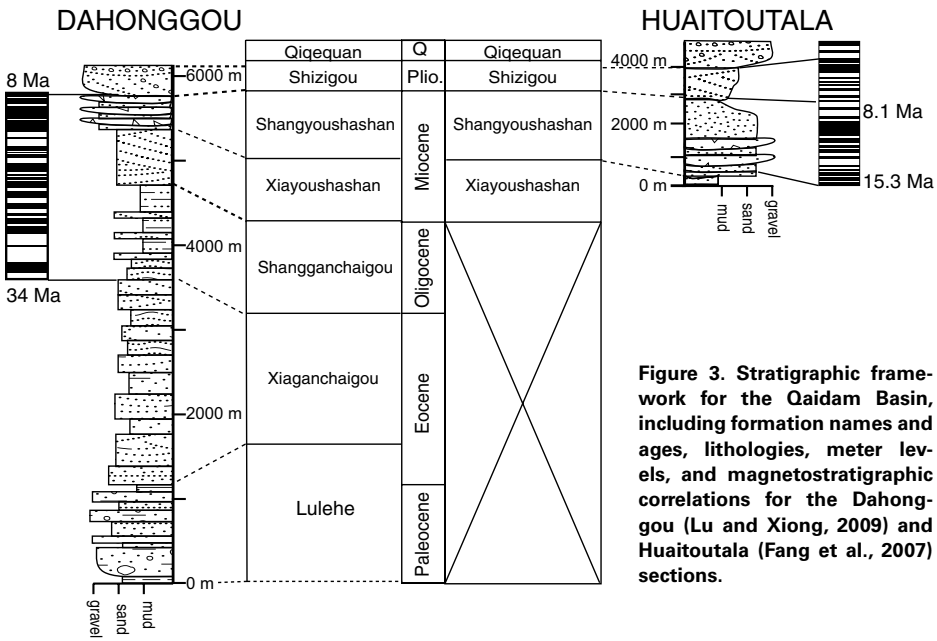


**Figure 3. Stratigraphic framework for the Qaidam Basin, including formation names and ages, lithologies, meter levels, and magnetostratigraphic correlations for the Dahonggou (Lu and Xiong, 2009) and Huaitoutala (Fang et al., 2007) sections.**

the upper part of the section to between 34 Ma and 8 Ma and have provided documentation of general lithologic trends of upper stratigraphic levels (Lu and Xiong, 2009; Zhuang et al., 2011).

## POTENTIAL SEDIMENT SOURCES

Potential sediment sources include mountain ranges surrounding the Qaidam Basin on all flanks (Fig. 2). Buried sedimentary and metamorphic units form the Qaidam basement, which could also have provided sediment during early basin filling. Next, we highlight the characteristic crystallization ages, lithologies, and heavy mineral constituents of each of these sources.

### Southern Sources

Along the southern basin margin, the Eastern Kunlun Shan east of ~92°E (Figs. 1 and 2) is principally composed of Permian–Middle Triassic (260–210 Ma) plutons with isolated lower Paleozoic granitic rocks (450–380 Ma; Fig. 5C; Harris et al., 1988; Roger et al., 2003; Mo et al., 2007; Pullen et al., 2008; Yuan et al., 2009; McRivette, 2011; J.Y. Zhang et al., 2012) intruding late Proterozoic to Paleozoic metamorphic basement rock. Heavy minerals associated with magmatic and metamorphic basement (pyroxene, hornblende, epidote, garnet) are expected from the Kunlun Shan and Qimen Tagh (L. Li et al., 2015). In contrast to the East Kunlun Shan, early Paleozoic (513–420 Ma) subduction-related intrusions occupy the Qimen Tagh (W. Li et al., 2013). Farther south, gneissic basement rocks north of the Kunlun fault yield Paleoproterozoic ages (Zhang and Zheng, 1994). Upper Carboniferous to Lower Permian shallow-marine sedimentary and volcanic strata are unconformably overlain by Jurassic–Cenozoic nonmarine strata (Mock et al., 1999). Southeast of the Kunlun Shan, there is the Songpan-Ganzi Basin (Fig. 1), a belt of Middle–Upper Triassic deep-marine clastic deposits with a broad mixture of Permian–Triassic, middle Paleozoic, and rare Precambrian detrital zircon age populations (Fig. 5A) from the North China block, South China block, Kunlun, and Qiangtang terranes (Weislogel et al., 2006, 2010; Weislogel, 2008; Enkelmann et al., 2007; Ding et al., 2013).

Directly south of the Eastern Kunlun Shan, the Hoh Xil Basin contains Cenozoic siliciclastic rocks characterized by Neoproterozoic, Paleozoic, and Permian–Triassic sources (Fig. 5B) derived from the Lhasa and Qiangtang terranes, as well as the Eastern Kunlun Shan (Dai et al., 2012; Staisch et al., 2014).

### Eastern Sources

To the east, Proterozoic metamorphic basement, Paleozoic–Mesozoic sedimentary and metasedimentary units, and Permian–Triassic granitoids are exposed in the Ela Shan and Dulan-Chaka highland (Fig. 2). These ranges divide the Qaidam Basin from Cenozoic intermontane basins of northeastern Tibet. Basement is composed of early Proterozoic high-grade metamorphic rocks, Paleozoic–Mesozoic sedimentary and low-grade metamorphic rocks, and extensive Permian–Triassic igneous bodies (Fig. 5G; Liu et al., 2004; Wu et al., 2004; Chen et al., 2012; Duvall et al., 2013).

### Western Sources

The Altyn Shan to the west of Qaidam Basin includes Archean–lower Paleozoic magmatic arc, accretionary prism, and related sedimentary successions. The Altyn Tagh fault (Figs. 1 and 2), which bisects the Altyn Shan, is a 1600-km-long left-lateral fault. Sedimentary units exposed in the Altyn Shan include Neoproterozoic quartz arenite and marbleized stromatolitic limestone (Gehrels et al., 2003a). Paleoproterozoic (1.6–2.0 Ga), Neoproterozoic (922–928 Ma), Ordovician–Silurian (430–480 Ma), and Permian (260–280 Ma) zircon U-Pb ages are common in igneous and metamorphic basement of the Altyn Shan (Fig. 5F; Gehrels et al., 2003b).

### Northern Sources

Finally, north of the basin, localized ultrahigh-pressure metamorphic complexes, magmatic arcs, and recycled sedimentary units comprise the northern Qaidam and Qilian Shan–Nan Shan region (QBGMR, 1991). These sedimentary and magmatic units are underlain by Proterozoic and Archean crystalline basement (Yin and Harrison, 2000; Gehrels et al., 2003a, 2003b). The Qilian Shan–Nan Shan (Figs. 1, 2, and 5D) includes the North Qaidam terrane of Proterozoic gneiss overlain by Paleozoic metasedimentary rocks (QBGMR, 1991). Early Paleozoic arcs developed along the southern margin of the North China craton (Yin and Harrison, 2000; Xiao et al., 2009), including marine sedimentary rocks, ophiolites, and ultrahigh-pressure metamorphic complexes (Menold et al., 2009; Xiao et al., 2009). Heavy mineral provinces of the southern Qilian Shan–Nan Shan can be expected to contain high volumes of epidote, hornblende, garnet, rutile, and metamorphic accessory minerals such as kyanite, andalusite, and sillimanite. The Qilian Shan–Nan Shan contains isolated Permian–Triassic plutons (Chen et al., 2012). Silurian–Ordovician strata are dominated by 450–490 Ma U-Pb ages from a local volcanic source and a minor Proterozoic component (Gehrels et al., 2011). In addition, recycling of Mesozoic and late Paleozoic sedimentary units would provide Permian–Triassic-aged zircons, such as the unimodal 270–280 Ma population observed in Jurassic sandstones associated with magmatic ages in the Kunlun arc (Yan et al., 2010; Gehrels et al., 2011).

### Local Basement Sources

Neoproterozoic and lower Paleozoic metamorphic rocks, flysch, and carbonates form part

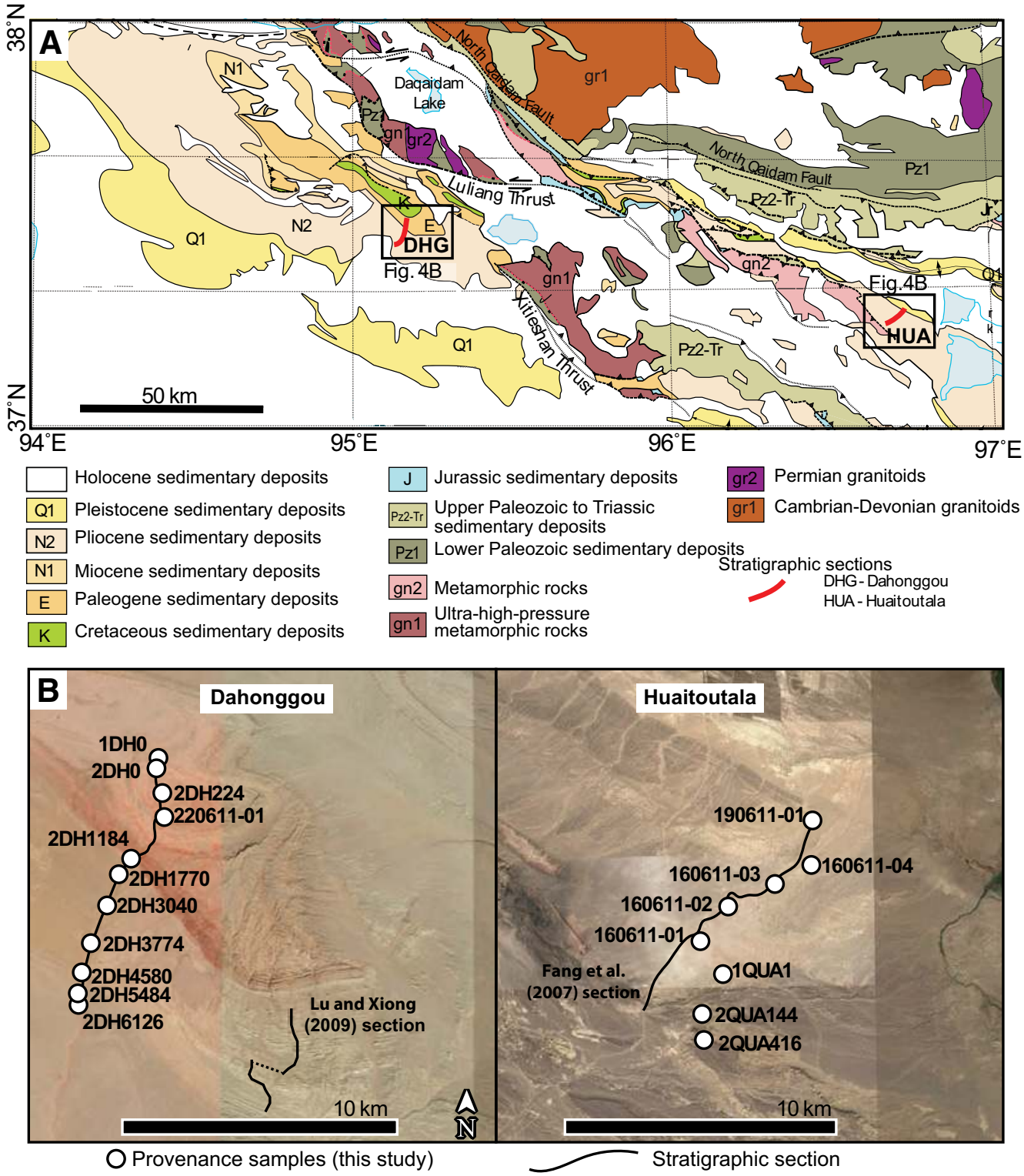


**Figure 4. (A) Geologic map of the northern margin of the Qaidam Basin (modified from Yin et al., 2008a) showing localities for this study. (B) Satellite images of Dahonggou and Huaitoutala localities, with measured section traces (this study; Fang et al., 2007; Lu and Xiong, 2009) and provenance sample locations.**

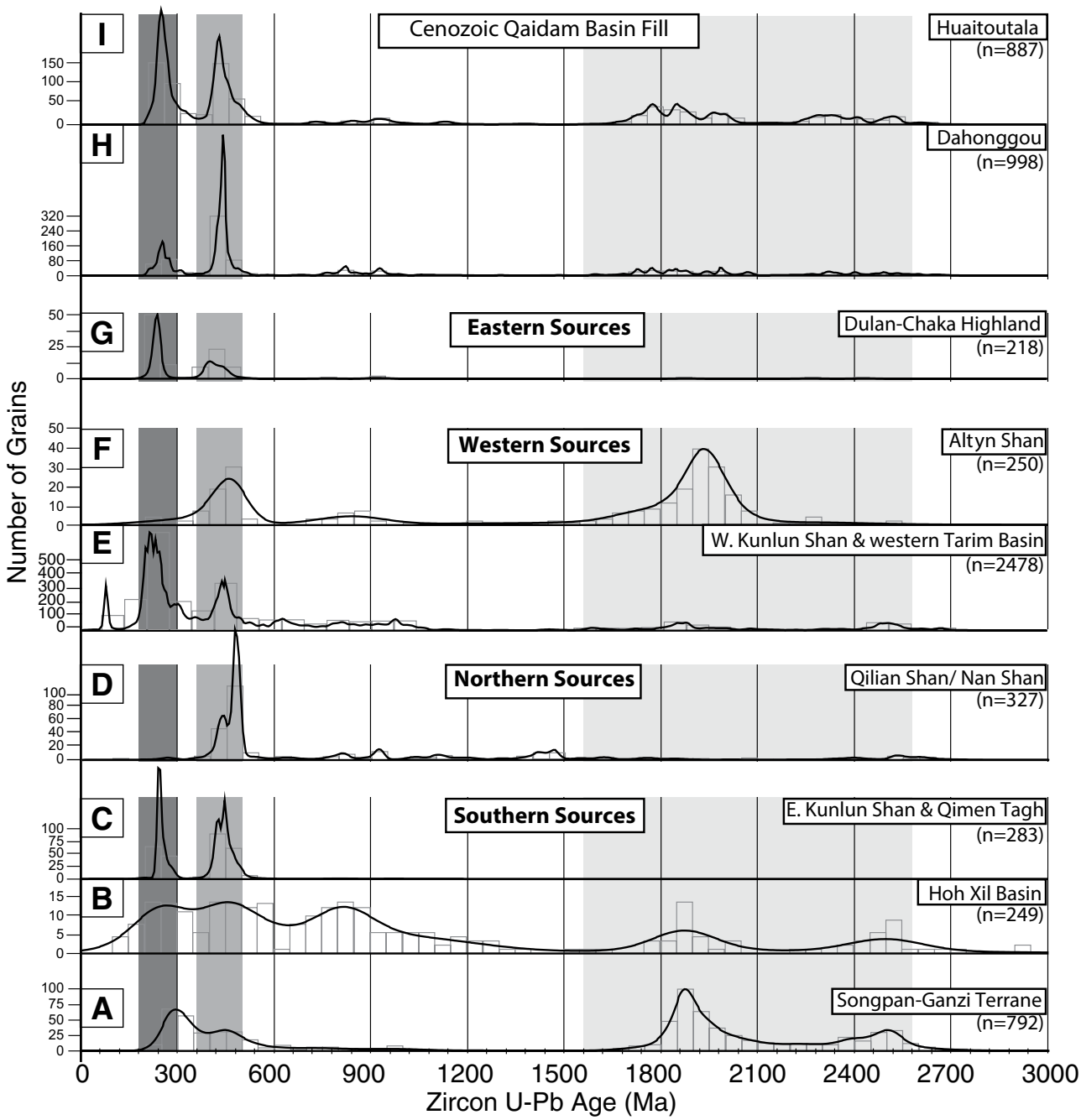


**Figure 5. Histograms and kernel density estimates for source area detrital and magmatic zircon U-Pb age data. Gray vertical bars indicate the major populations identified in Cenozoic Qaidam Basin fill in this study. (A) Songpan-Ganzi Basin (Weislogel et al., 2010). (B) Hoh Xil Basin (Dai et al., 2012). (C) Eastern Kunlun Shan and Qimen Tagh (Cowgill et al., 2003; Pullen et al., 2011; W. Li et al., 2013). (D) Western Kunlun Shan and western Tarim Basin (Bershaw et al., 2012; Robinson et al., 2012; Carrapa et al., 2014). (E) Qilian Shan–Nan Shan, and North Qaidam (Cowgill et al., 2003; Gehrels et al., 2003a, b; Menold, 2006; Yan et al., 2010). (F) Altyn Shan (Cowgill et al., 2003; Gehrels et al., 2003a, b). (G) Dulan-Chaka highland (Liu et al., 2004; Wu et al., 2004; Chen et al., 2012). (H) All Dahonggou samples from this study. (I) All Huaitoutala samples from this study.**

of the Qaidam basement beneath Mesozoic–Cenozoic basin fill (Wang and Coward, 1990; Xia et al., 2001; Chen et al., 2012). Jurassic–Cretaceous nonmarine rocks exposed on the northern Qaidam margins and in well logs (QBGMR, 1991) were sourced from early exhumation in the Qilian and Altyn Shan (Ritts and Biffi, 2001; Sobel et al., 2001; Gehrels et al., 2003b).

## SEDIMENTOLOGY AND DEPOSITIONAL ENVIRONMENTS

We recognize major depositional shifts based on facies distributions of six formations (Fig. 6). Initial coarsening (Lulehe) was followed by fining (Xiaganchaigou), continued fining and transition from fluvial to marginal lacustrine deposits (Shangganchaigou), and final coarsening (Xiayoushashan, Shangyoushashan, and Shizigou).

### Lulehe Formation

#### *Description*

Fine-grained, distinctively red deposits of the lower Lulehe Formation (0–220 m) are characterized by trough cross-stratified and horizontally bedded sandstone (Fig. 7A) with laminated mudstone lenses and pebble lags above sharp bases (Fig. 8F). Fine- to medium-grained sandstone packages contain downstream accretion surfaces and are typically 3–7 m thick and 10–20 m wide with lenticular geometries. These fine upward into mudstone intervals up to 3 m thick, which feature mottling and variable destruction of primary sedimentary structures.

The upper Lulehe Formation (220–1100 m) contains 1–5-m-thick lenticular beds of polymict, poorly sorted, clast-supported, granule-cobble conglomerate interbedded with medium- to coarse-grained, trough cross-stratified sandstone (Figs. 7B and 8A). Conglomerate beds have sharp erosional surfaces incising up to 1 m into underlying beds and a matrix of poorly sorted, calcite-cemented sandstone. These beds pinch out laterally, fine upward to coarse-grained sandstone, and include horizontally stratified, imbricated, and structureless varieties. Overlying conglomerate beds are horizontally laminated or structureless red mudstone beds 2–5 m thick (Fig. 8H).

#### *Interpretation*

Lower Lulehe levels represent a moderate-energy fluvial system with stable floodplains. The sharp bases, gradational upper surfaces, and low width-to-thickness ratios of the sandstones are similar to sand bodies typical of channel-fill deposits (e.g., Friend et al., 1979; Tornqvist, 1993). Structureless red mudstones are interpreted as overbank deposits with subaerial exposure and pedogenesis. Trough cross-stratified sandstone bodies, stable overbank deposits, and lack of laterally accreting bar forms are consistent with a low-sinuosity channel belt in a sandy, low- to moderate-gradient braided or anastomosing fluvial system with multiple channels, downstream accreting bar forms, and vertical aggradation (Cant and Walker, 1978; Ethridge et al., 1999; Makaske, 2001). We interpret the increase in grain size and sand-to-mud ratio in the upper 20 m of this interval as a transition to a higher-competence fluvial system.

Upper Lulehe conglomerate beds preserve channel thicknesses 1–5 m thick (Fig. 7B). Clast support, imbrication, poor sorting, coarse grain size, and scoured bases indicate deposition by a higher-energy system (Nemec and Steel, 1984; Smith, 1990). Structureless and horizontally stratified conglomerate beds are considered components of downstream-migrating compound bars (Miall, 1977). This interval is consistent with a transition to a higher-gradient gravelly braided fluvial system, although the presence of mudstone beds indicates highly variable flows.

### Xiaganchaigou Formation

#### *Description*

The intermediate succession (1100–3550 m) contains finer material with few gravel clasts (Fig. 7C). The deposits consist of multistory sand bodies in 5–10-m-thick packages with sharp bases, commonly fining upward in the basal 50 cm; these are composed of 5–10-cm-thick beds of horizontally and ripple cross-stratified, fine- to very fine-grained silty sandstone (Fig. 8B). The packages contain mudstone drapes and interbeds and are capped by 1–3-m-thick mudstone intervals displaying blocky soil aggregates (peds), pedogenic slickensides, carbonate nodules, red and green mottling, rhizoliths, and moderate bioturbation.

Above 1250 m, interbedded sandstone and mudrock deposits dominate, featuring upward-coarsening and upward-thickening intervals of laminated mudstone and massive to horizontally stratified, laterally continuous sandstone sheets 0.5–2 m thick (Fig. 8C). In sharp contact with these interbedded deposits, trough cross-stratified, medium-grained sandstone packages reach 20–40 m (up to 75 m) in thickness (Fig. 8I). These thick sandstone packages persist to ~3550 m, with mudstone intervals increasing above the ~3000 m level.

#### *Interpretation*

Upward-fining mudstone, cross-bedded sandstone, and interbedded paleosols represent a fine-grained fluvial system with pedogenically modified overbank settings. Trough cross-stratified sandstones indicate dune migration, with laminated mudstones resulting from low-flow isolation of dunes and mud deposition (Smith, 1990). Stability of the surrounding floodplain is suggested by ubiquitous root traces, mottling, and soil structures. The lack of distinctive soil profiles points to aggradational alluvial soils (Besly and Fielding, 1989). Thick sandstone bodies are typical of amalgamated channels in a high-sinuosity channel belt; upward-coarsening and upward-thickening mudstone and sandstone intervals represent crevasse splays. These overbank, channel margin, and in-channel deposits are considered representative of a meandering fluvial system (e.g., Nanson, 1980; Kraus, 1996).

### Shangganchaigou Formation

#### *Description*

The Shangganchaigou (3550–4805 m) shows continued fining and is dominated by laminated mudstone and ripple-laminated fine-grained sandstone (Fig. 7D). Thin beds (0.5–2 m) of mottled, nodular mudstone coarsen upward into fine-grained structureless or cross-laminated sandstone (Fig. 8K). These thinly bedded heterolithic deposits are commonly incised by upward-fining, lenticular cross-laminated sandstone bodies. Cross-laminae are generally asymmetric, with occasional symmetrical cross-laminae (Fig. 8C). Rare lateral accretion surfaces in sandstone beds are less than 1 m thick.

#### *Interpretation*

The thin-bedded sandstone and laminated to structureless mudstone of this association are attributed to floodplain deposition, based on upward-coarsening packages and association with channel sandstones (Porter and Gallois, 2008). Mudstone packages capping channel sandstones indicate phases of channel abandonment. Lack of lacustrine ichnofacies, freshwater fish fauna (Wang et al., 2007), soft sediment deformation, and lacustrine carbonate or beach facies helps rule out an open lacustrine setting, though such facies are identified in the distal basin (Zhuang et al., 2011). These deposits likely represent an alluvial plain with splays into shallow ephemeral lakes, as expressed by bidirectional ripples and thick mudstone packages.

### Xiayoushashan, Shangyoushashan, and Shizigou Formations

#### *Description*

Upper stratigraphic levels (4805–6200 m) comprise the second major coarse-grained interval (Fig. 7E). Deposits are dominated by normally graded, trough cross-stratified conglomerate and medium- to very coarse-grained

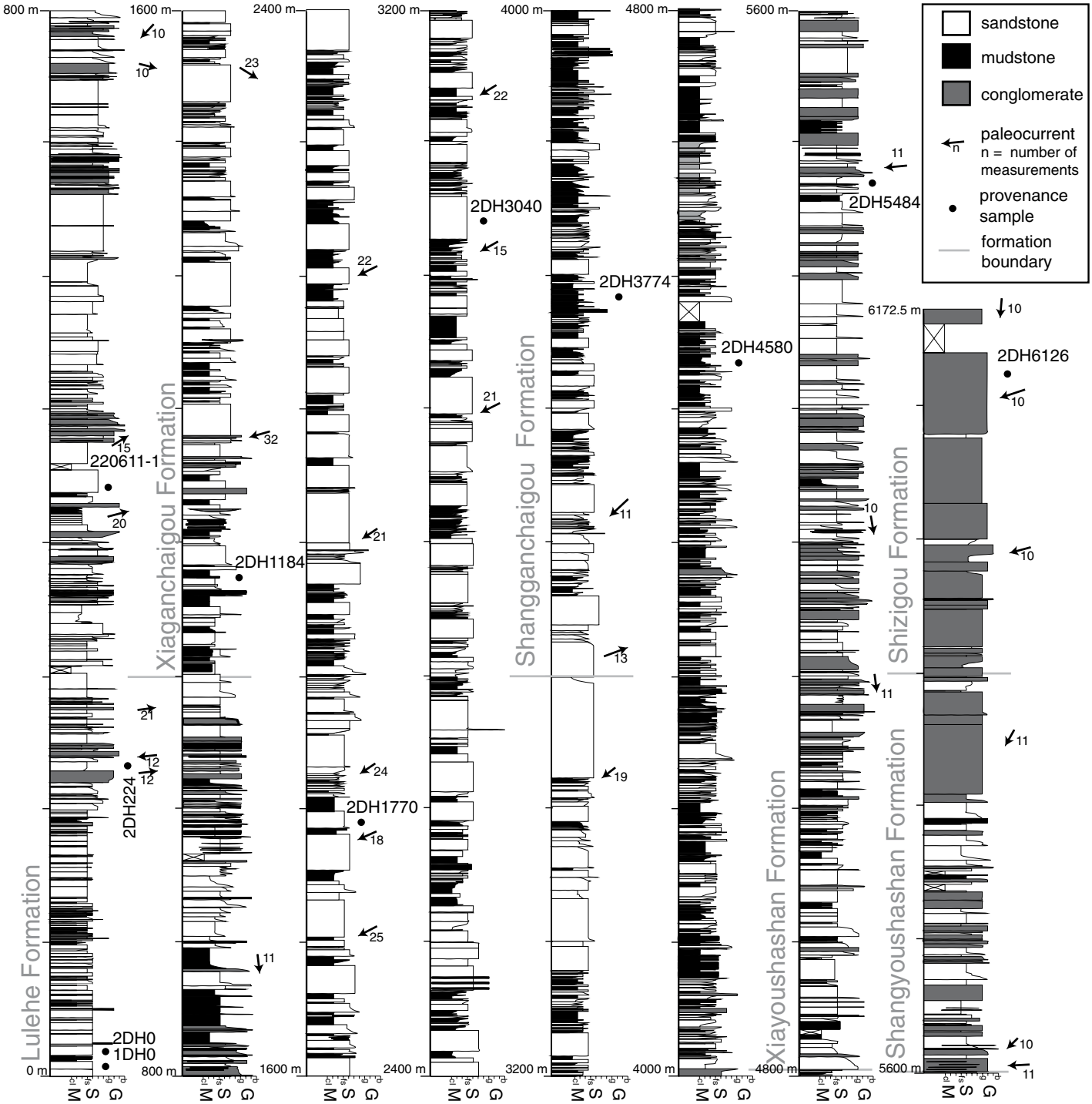


**Figure 6. Measured stratigraphic section at the Dahonggou anticline, with paleocurrent orientations and provenance sample locations. For lithology column, M, S, and G represent mudstone, sandstone, and conglomerate; cl, fs, g, b represent clay, fine sand, gravel, boulder, respectively.**

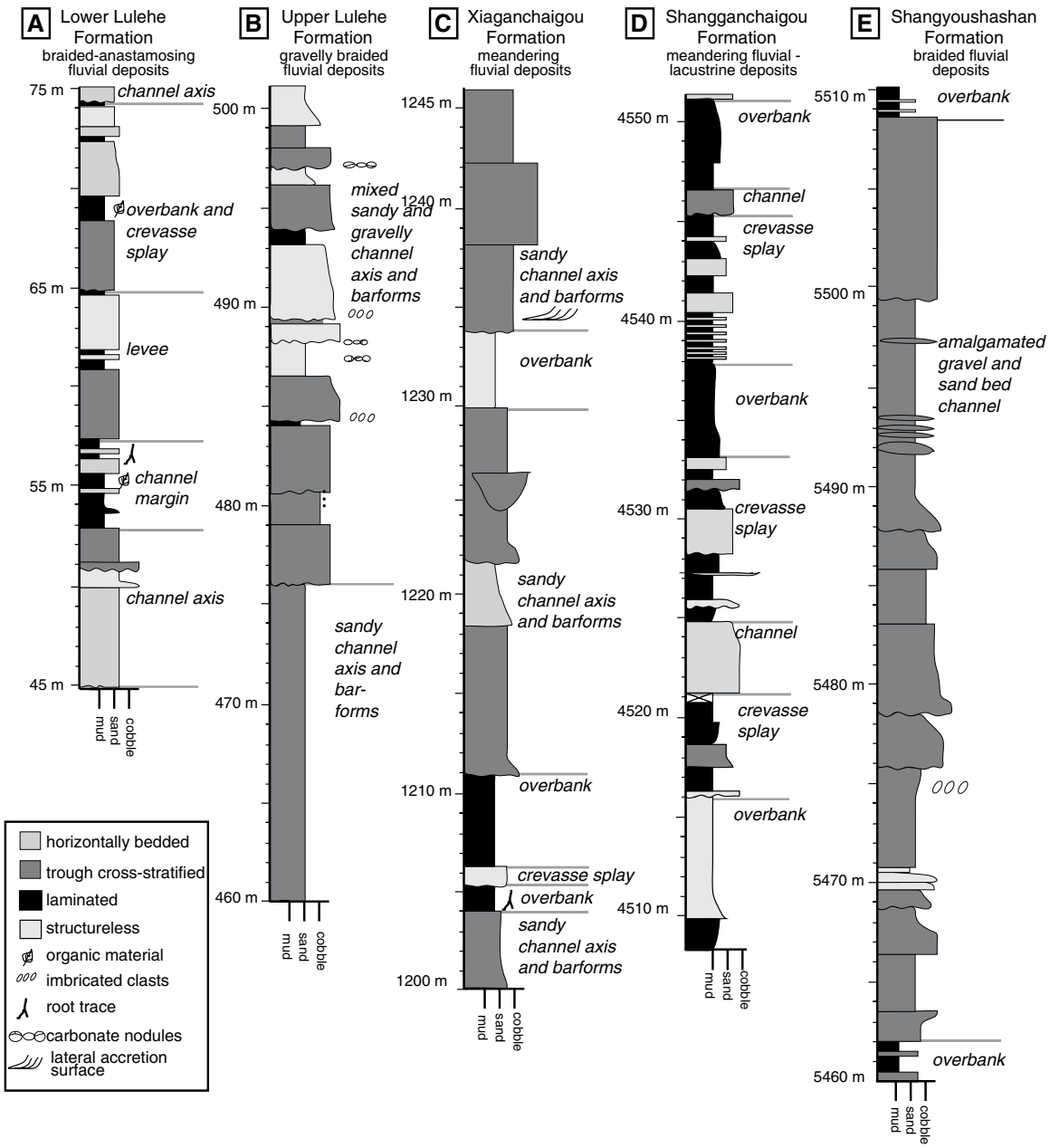


**Figure 7. Representative stratigraphic columns for major depositional environments of the Dahonggou section. (A) Braided-anastomosing fluvial deposits of the lower Lulehe Formation. (B) Gravelly braided fluvial deposits of the upper Lulehe Formation. (C) Meandering fluvial deposits of the Xiaganchaigou Formation. (D) Meandering fluvial-lacustrine deposits of the Shangganchaigou Formation. (E) Braided fluvial deposits of the Shangyoushashan Formation.**

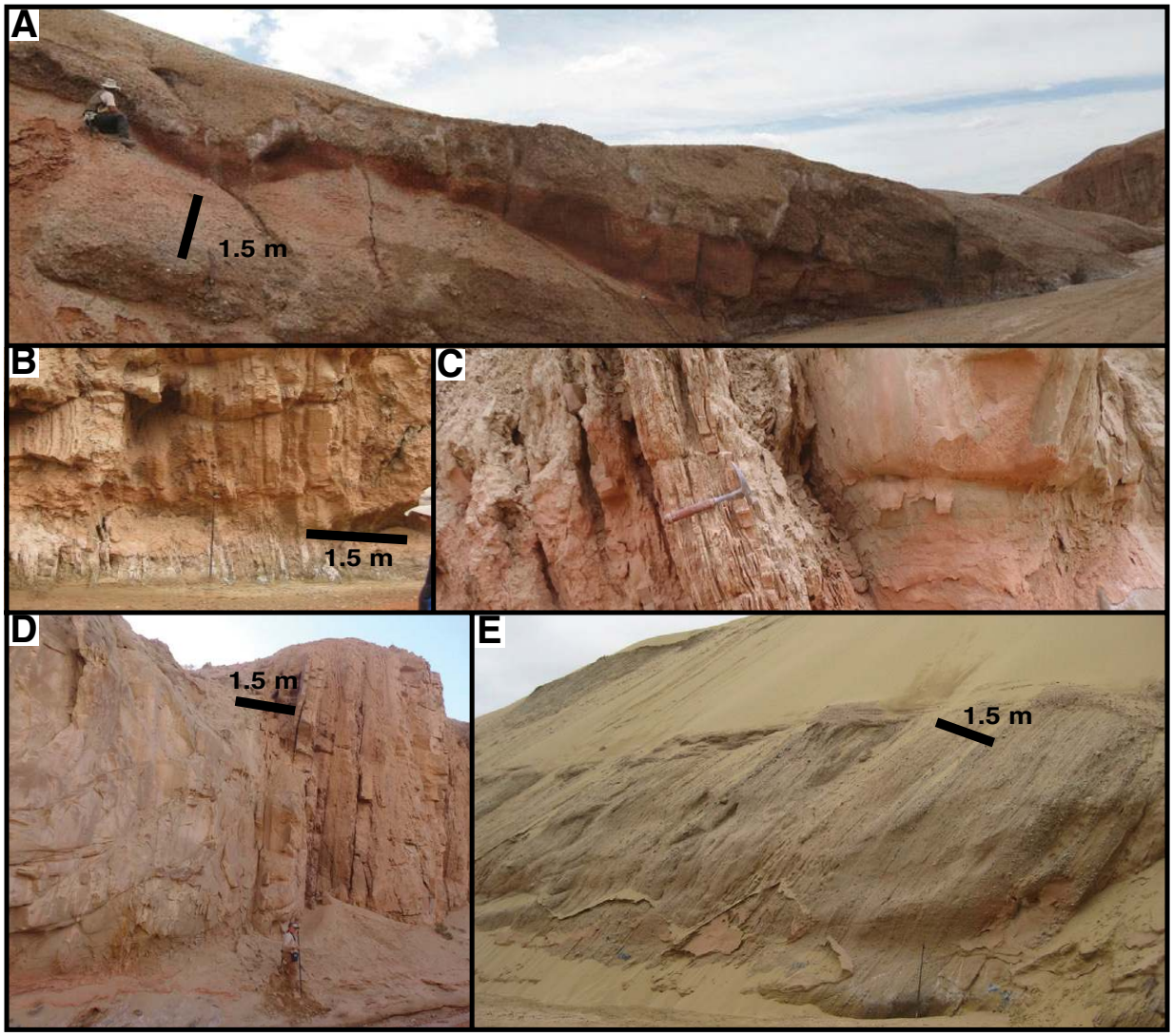


**Figure 8 (*on this and following page*). Field photographs of lithofacies and stratigraphic units at the Dahonggou section. Stratigraphic levels refer to Figure 6. (A) Erosive, laterally continuous conglomerate beds interbedded with structureless mudstone and sandstone. Lulehe Formation, 480 m. (B) Interbedded sandstone and mudstone. Sandstone package thickness and frequency increase upward. Xiaganchaigou Formation, 1940 m. (C) Structureless, red and green mottled mudstone. 1–10 cm beds of ripple cross-stratified and horizontally laminated fine-grained sandstone increase in thickness up to a sharp contact with trough cross-stratified medium-grained sandstone bed. Xiaganchaigou Formation, 2970 m. (D) Thick package of trough cross-stratified sandstone capped by interbedded mudstone and sandstone. Xiaganchaigou Formation, 3200 m. (E) Trough cross-stratified pebble conglomerate and medium- to coarse-grained sandstone. Shangyoushashan Formation, 5965 m. (F) Amalgamated trough cross-stratified sandstone overlying laminated red mudstone. Lulehe Formation, ~50 m. (G) Interbedded coarse-grained cross-bedded sandstone and clast-supported pebble conglomerate, Lulehe Formation, 489 m. (H) Structureless to laminated red mudstone incised by trough cross-stratified clast-supported pebble conglomerate. Lulehe Formation, 815 m. (I) Two amalgamated channel complexes separated by interbedded sandstone and mudstone. Xiaganchaigou Formation, 2800 m. Up section is to the right. (J) Bidirectional current ripple cross-stratification. Shangganchaigou Formation, 4523 m. (K) Upward-coarsening packages of sandy siltstone to fine sandstone. Shangganchaigou Formation, 3659.7 m. (L) Horizontally bedded clast-supported pebble-cobble conglomerate interbedded with coarse- to very coarse-grained sandstone. Shangyoushashan Formation, 5603 m.**

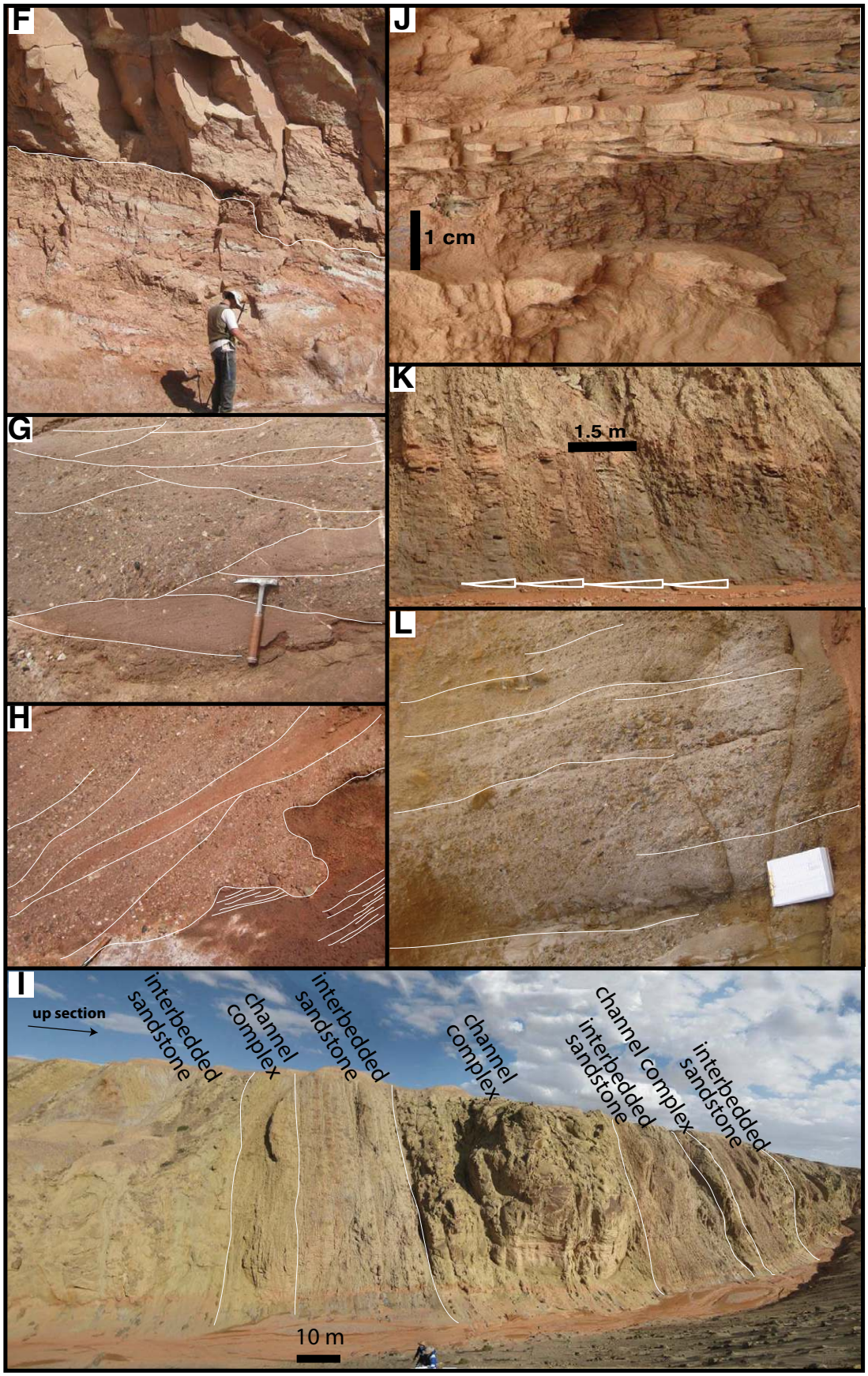

sandstone (Fig. 8E). Beds are 1–4 m thick, with sharp bases and lenticular geometries (Fig. 8L). At 4800–5800 m, <1-m-thick beds of mottled, structureless siltstone are interbedded with fine- to very fine-grained, structureless to ripple cross-laminated sandstone. The frequency and thickness of granule-pebble conglomerate beds increase up section (4805–5787 m), with capping deposits (above 5787 m) dominated by clast-supported, planar to trough cross-stratified, imbricated conglomerate containing sandstone lenses and clasts up to 1 m in diameter.

#### *Interpretation*

Lithofacies and stratal geometries are characteristic of a sandy to gravelly braided fluvial system (Rust, 1972; Cant and Walker, 1978). Normally graded, trough cross-stratified, clast-supported conglomerates are consistent with dune migration in fluvial channels during flood and waning flow conditions (Miall, 1977). The absence of matrix-supported debris-flow conglomerates and sandy sheetflood deposits precludes a proximal alluvial-fan setting. Coarse grain size, cross-stratification, erosive bases, and lenticular bed geometries are representative of proximal deposition in an aggradational, low-sinuosity channel belt. The upward-thickening and upward-coarsening pattern likely indicates a progradational system in which coarse-grained transverse fluvial systems advanced into the basin.

### Regional Evolution of Depositional Systems

Shifting depositional systems are evidenced by facies variations and grain-size trends in the Dahonggou section, consistent with other studies of Cenozoic strata across the basin (e.g., Bally et al., 1986; Hanson et al., 2001; Zhuang et al., 2011). Coarse intervals represent basinward progradation, potentially linked to climate change and/or deformation shifts in source regions, or reduced accommodation in proximal basin settings. Fine intervals may represent changing basin architecture in response to differential subsidence, cutoff of basin outlets and resulting internal drainage, and/or varying sediment discharge in response to changes in climate, source lithologies, and drainage divide position.

The first major shift is represented by the Eocene transition from a low-gradient fluvial system (lower Lulehe Formation) to coarse-grained braided river system (upper Lulehe Formation). The red color, palynologic data (Miao et al., 2008), and weathering indices (chemical index of alteration, plagioclase index of alteration, chemical index of weathering, and modified chemical index of weathering from Song et al., 2013b) are consistent with strong chemical weathering linked to a warm, wet climate. Similar deposits are observed along strike to the northwest at Lake Mahai and Lulehe (Fig. 2; Zhuang et al., 2011), suggesting regional drainage reorganization of a braided fluvial system.

The Xiaganchaigou Formation is characterized by thick multistory channel stacking within a lower-gradient, sandy fluvial system. These deposits can be correlated with coarser meandering fluvial deposits at the Lake Mahai and Lulehe sections (Fig. 2; Yin et al., 2008a, 2008b; Zhuang et al., 2011).

The Shangganchaigou Formation is composed of interbedded paleosol, channel belt, and marginal lacustrine deposits of a low-gradient fluvial system with small lake basins (Fielding, 1986; Miall, 2013). During this phase, the depocenter was situated in the western basin (Ganchaigou and Hongshanhan sections of Zhuang et al., 2011; Fig. 2), where laminated mudstones and evaporites indicate profundal and hypersaline lacustrine environments (Bally et al., 1986). Adjacent to the depocenter, there are marginal lacustrine clastic and calcareous mudstones, including subaerial mud cracks and subaqueous algal stromatolites, ostracods, and pisoliths (Hanson et al., 2001). During endorheic periods, a central evaporative lake was likely quite shallow, resulting in significant shoreline advance and retreat.

Miocene–Pliocene deposits are clast-supported conglomerate and coarse-grained trough cross-bedded sandstones of braided fluvial systems. The interval at Dahonggou exceeds 1000 m, but it thins to ~600 m at Lake Mahai (Zhuang et al., 2011). Upward coarsening and thickening of this conglomeratic succession are attributed to progradation of a proximal fluvial system, possibly a fluvial megafan (Horton and DeCelles, 2001) derived from a large hinterland catchment area in the southern Qilian Shan fold-thrust belt. This interval is coincident with a regional tectonic reorganization proposed for northeastern Tibet.

## SEDIMENT PROVENANCE

A multiproxy provenance approach (paleocurrent, sandstone petrographic, detrital zircon U-Pb geochronologic, and heavy mineral analyses) for the 6200-m-thick Dahonggou section (Figs. 4 and 6) helps to constrain topographic development of several ranges around the basin. To constrain lateral variability, U-Pb results are also presented for the 1400-m-thick Huaitoutala section, ~100 km to the E (Figs. 3 and 4), where Miocene and younger deposits (magnetostratigraphy from Fang et al., 2007) are exposed in the hanging wall of the Eastern Luliang, Xitie Shan, and Lenghu thrust system of the southern Qilian Shan–Nan Shan.

### Paleocurrent Analysis

Paleocurrents from 30 localities help to constrain dispersal patterns and indicate a major switch in paleoflow. At each locality, paleoflow was determined from measurements of at least 10 imbricated clasts or 15 trough limbs. Data (Fig. 9) show a major switch from E-directed flow for the lower Lulehe Formation (four sites, 220–500 m; Fig. 6) to principally SW-directed flow for upper sites (29 sites, 1100–6200 m; Fig. 6). Paleocurrents at the base of the section point to an axial fluvial system flowing from the west, eliminating the northeastern region as a primary source during the early Cenozoic. In contrast, SW-directed flow for upper levels is comparable to the modern configuration, revealing transverse dispersal away from the Qilian Shan–Nan Shan since the Eocene.

### Sandstone Petrography

Sixty-seven petrographic thin sections of medium-grained sandstone samples were examined, with 14 selected for point counting using the Gazzi-Dickinson method (Gazzi, 1966; Dickinson, 1970, 1985). These submature, moderately sorted feldspathic litharenites–litharenites (mean composition $Q_{63}Ft_{10}Lt_{27}$; Folk, 1980; Fig. 10) preserve unstable metamorphic rock fragments (range 3–18%, mean 11%) and heavy minerals including kyanite, sillimanite, garnet, zircon, and chlorite. Polycrystalline quartz with extensive grain-boundary migration is common. Sedimentary rock fragments are also common throughout the section (range 2–14%, mean 7%).

Petrographic data are comparable to sandstones from the same units in the western Qaidam Basin, though our samples contain a higher ratio of metamorphic to volcanic rock fragments (Rieser et al., 2005). Mesozoic sandstones from the northeastern basin are quartz- and feldspar-rich sandstones ($Qm_{62}F_{24}Lt_{14}$; Fig. 10), with fewer rock fragments (Ritts, 1998). Compositional data indicate recycled orogenic and collisional suture or fold-thrust belt sources (Fig. 10; Dickinson and Suczek, 1979). Sandstone compositions show a minor increase in the abundance of lithic grains between the Shangganchaigou and Xiaganchaigou Formations, followed by a return to slightly higher quartz content in the overlying Shangyoushashan Formation (Fig. 10). Ubiquitous and diverse rock fragments attest to the proximity and/or complex geology of the catchment, but they do not allow for identification of a specific source.

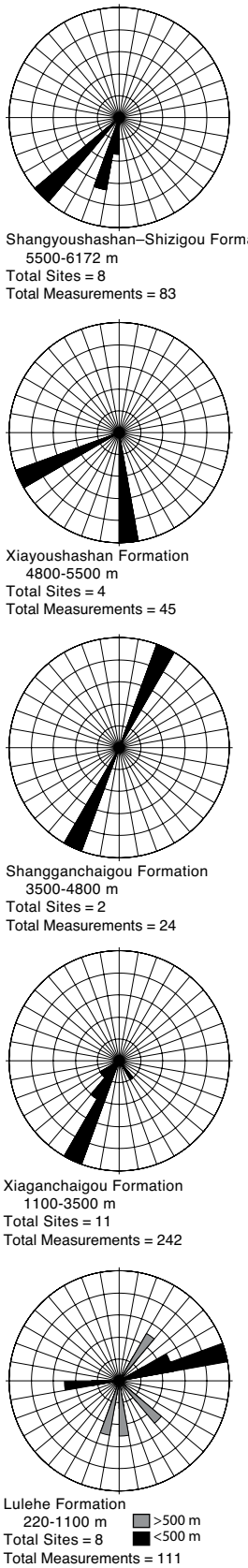


**Figure 9. Rose diagrams for paleocurrent data from Dahonggou section shown in Figure 6.**

## Detrital Zircon Geochronology

Detrital zircon U-Pb geochronologic analyses were employed to constrain Cenozoic sediment provenance for the Qaidam Basin. Shifts in detrital U-Pb ages allow discrimination among potential source areas and may be linked to changes in deformation patterns, shifting upstream drainage configurations, or unroofing of progressively deeper rock units.

### *Methods*

Detrital zircon U-Pb ages were obtained for 19 sandstone samples: 11 from Dahonggou and 8 from Huaitoutala. For each sample, ~5 kg of medium-grained sandstone were collected and processed according to standard mineral separation techniques. 120 zircon grains were randomly selected from the nonmagnetic heavy mineral fraction of each sample and analyzed by laser ablation–multicollector–inductively coupled plasma–mass spectrometry (LA-MC-ICP-MS) at the Arizona LaserChron Center at the University of Arizona, Tucson, Arizona. Analyses were conducted using a laser spot size of 30 μm, avoiding impurities, and using a Sri Lankan zircon standard for calibration according to Arizona LaserChron Center protocols (Gehrels et al., 2008, 2011). Errors in determining $^{206}Pb/^{238}U$, $^{206}Pb/^{204}Pb$, and $^{206}Pb/^{207}Pb$, result in a measurement error of ~1–2% (at 2σ level), but this can be substantially larger for grains younger than 1.0 Ga due to low intensity of the $^{207}Pb$ signal. The $^{206}Pb/^{238}U$ ages are reported for grains with $^{206}Pb/^{238}U$ ages younger than 900 Ma, whereas $^{206}Pb/^{207}Pb$ ages are reported for older grains. Only ages with <20% discordance or <5% reverse discordance were considered robust enough for interpretation. Analytical results (Table DR1[1]) consist of 1999 analyses for 19 samples and are presented as age histograms and kernel density estimates (Fig. 11A) using the DensityPlotter routine outlined by Vermeesch (2012).

### *Results*

U-Pb results help to constrain Cenozoic sediment provenance. Major populations in the Qaidam Basin samples include: (1) Permian–Triassic (299–200 Ma), (2) Late Cambrian to Early Devonian (500–400 Ma), and (3) Paleoproterozoic (2.5–1.6 Ga).

At the base of the section, two lower Lulehe Formation samples (1DH0 and 2DH0) display a bimodal distribution, with peaks at 250 Ma and 436 Ma, and rare Proterozoic grains. Up section, two upper Lulehe Formation samples (2DH224 and 220611-01) yield a unimodal early Paleozoic peak of ca. 440 Ma, a departure from samples below (2DH0) and above (2DH1184). Though rare, there is a significant increase in Proterozoic zircons in upper Lulehe Formation samples (2DH224 and 220611-01). Three Xiaganchaigou Formation samples (2DH1184, 2DH1770, 2DH3040) show diverse zircon age spectra with peaks corresponding to the three aforementioned age populations, including the initial appearance of Late Triassic crystallization ages. Contrasting detrital zircon age spectra are revealed for two Shangganchaigou Formation samples (2DH3774, 2DH4580). Minor Precambrian peaks are present in both samples, though their frequency increases significantly at 2DH4580, continuing to the top of the section. The remaining 10 samples from the Dahonggou and Huaitoutala sections, from the Xiayoushashan, Shangyoushashan, and Shizigou Formations (from Dahonggou: 2DH5484, 2DH6126; from Huaitoutala: 1QUA1, 2QUA144, 2QUA416, 160611-01, 160611-03, 160611-02, 160611-01, 190611-01), contain all three major age populations.

The *D* value of the Kolmogorov-Smirnov test (K-S test) was used to compare detrital zircon U-Pb age cumulative distribution functions, and to determine the probability that samples are derived from the same parent population. The K-S test *D* value is calculated as the maximum absolute difference between two samples' empirical cumulative distribution function and is a measure of the dissimilarity between two samples. Multidimensional scaling was then used to create a spatial visualization or "map" (Fig. 11B) of the dissimilarity measure (Vermeesch, 2013). Three groups of similarly sourced samples were identified using this metric: (1) 1DH0 and 2DH0, both displaying a zircon assemblage consisting of both early Paleozoic and Permian–Triassic ages, (2) 2DH224, 220611-01, and 2DH3774, which are dominated by a single early Paleozoic population, and (3) the remaining samples, which contain a cosmopolitan assemblage of all major detrital zircon populations (Fig. 11B).

## Heavy Mineral Analysis

Further discrimination of sources was obtained through heavy mineral (density > 2.89 g/cm$^3$) analyses for sandstones from the Dahong-

[1]GSA Data Repository Item 2015362, Table DR1. Sample locations, U-Pb isotopic results with 1σ uncertainties (rejected data in red italicized font), heavy mineral abundance data, sandstone petrographic point count data and paleocurrent measurement; Figure DR1. Concordia diagrams for all samples used in this study plotted using the Isoplot routine of Ludwig (2003), is available at www.geosociety.org/pubs/ft2015.htm, or on request from editing@geosociety.org.

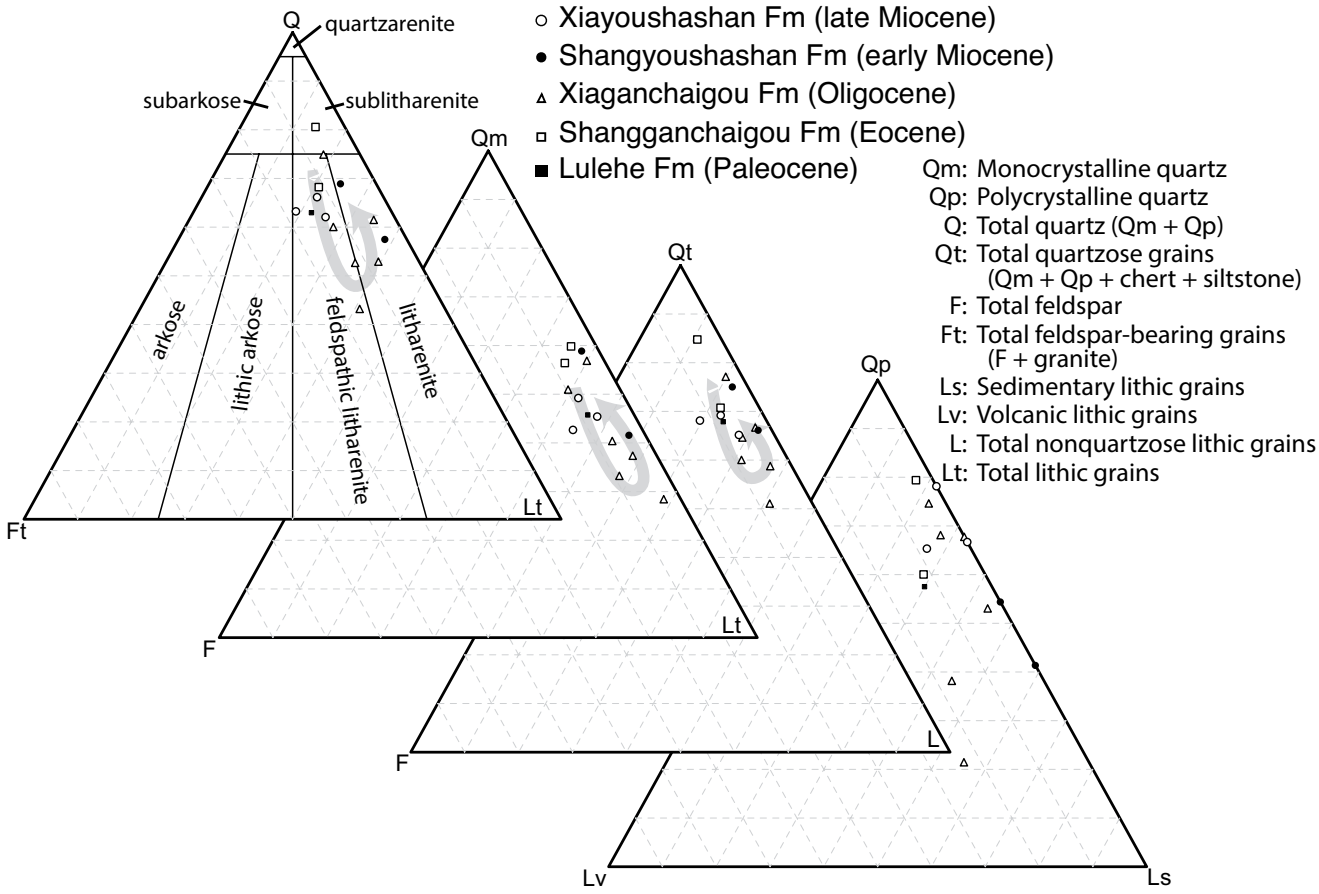


**Figure 10. Ternary diagrams of sandstone petrographic data. Light-gray arrow highlights an up-section decrease in maturity between the Shangganchaigou and Xiaganchaigou Formations, followed by a return to more mature sandstone compositions between the Xiaganchaigou and Shangyoushashan Formations. Fields for the leftmost ternary diagram are from Folk (1980). Ternary diagrams were created using Ternplot (Zahid and Barbeau, 2011).**

gou section. Heavy minerals generally constitute a minor volume, but they are a useful tracer of source evolution in orogenic belts and stratigraphic shifts in provenance (Mange and Maurer, 1992). Distinct petrologic characteristics of the Qilian Shan–Nan Shan and Kunlun Shan make heavy mineral analysis an important tool for understanding Qaidam Basin provenance.

### *Methods*

Ten heavy mineral fractions were separated from the same Dahonggou samples used for detrital zircon geochronology and analyzed using automated scanning electron microscopy (QEMSCAN) at the Colorado School of Mines, Golden, Colorado. Four energy dispersive X-ray (EDX) spectrometers acquired spectra from each particle with a beam stepping interval of 15 µm, an accelerating voltage of 25 keV, and a beam current of 5 nA; results were analyzed using the control program (iDiscover, FEI). Backscattered electron (BSE) values and EDX spectra were compared with previously determined values and spectra for a representative catalog of diverse mineral phases, facilitating a compositional assignment for each acquisition point and generation of a compositional map for each mount. This approach reflects the instrument design, which is optimized for rapid mineral identification rather than detailed intragranular compositional analysis (for which other techniques are more appropriate).

### *Results*

Results of QEMSCAN heavy mineral analyses revealed three groups with distinct assemblages (Fig. 12). In order to compare heavy mineral assemblages, the index ratios ZTR (zircon-rutile-tourmaline; Hubert, 1962), ATi (apatite-tourmaline index), RZi (rutile-zircon index), and MZi (monazite-zircon index; Morton and Hallsworth, 1994) were used, comparing minerals of similar weathering and diagenetic stability, and hydraulic behavior. In addition, volume percent of each heavy mineral species was calculated for each sample.

Lulehe Formation samples (1DH0, 2DH0, and 2DH224) contain a high volume percent of epidote (average 23.29) with increasing hornblende (average 18.95, increasing from 14.68 to 26.70) and tourmaline (average 0.12, increasing from 0.06 to 0.12). The highest GZi (98.07) and lowest ATi (80.93) are in this group. Whereas alumino-silicate metamorphic accessory minerals andalusite, kyanite, and sillimanite are absent from this sample, these minerals are susceptible to dissolution and/or replacement due to both metamorphic and sedimentary processes. The association of epidote and hornblende, low volume percent of sphene (average 3.29), orthopyroxene (average 0.02), and monazite (average 0.02), and high GZi/ATi ratio (82.5) suggest a source terrane dominated by greenschist-facies metamorphic rocks.

Xiaganchaigou samples (2DH1184, 2DH1770, and 2DH3040) show a significant departure from Lulehe heavy mineral assemblages. There is a switch to low epidote (average 7.78) and hornblende (average 4.93), and

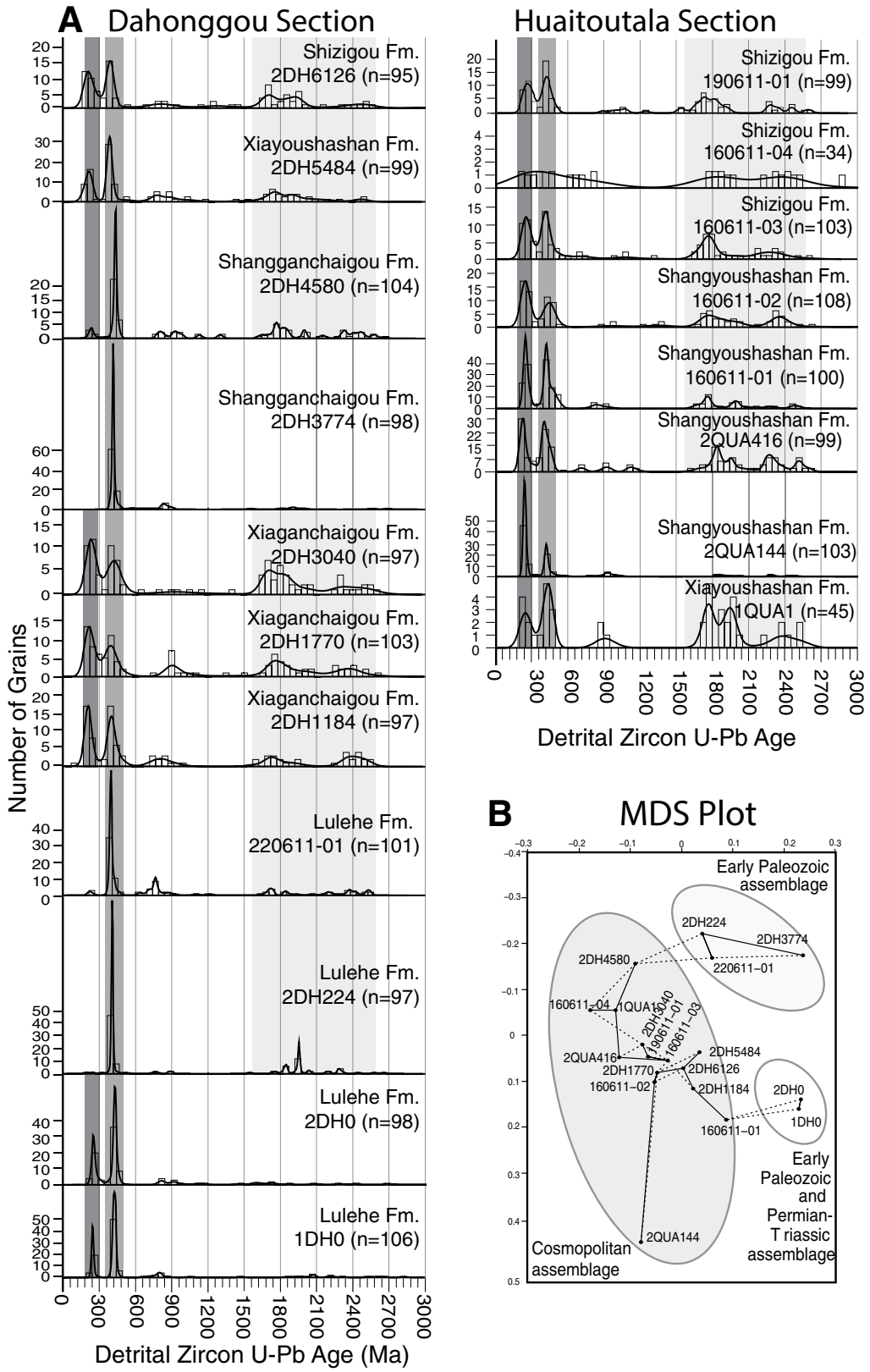


**Figure 11. (A) Kernel density estimates and histograms for detrital zircon U-Pb age data showing geochronologic results for 11 samples from the Dahonggou section and eight samples from the Huaitoutala section (locations shown in Figs. 2 and 5). Samples are presented in stratigraphic order and grouped by locality. Shaded bars indicate the presence or absence of major source populations—Permian–Triassic; early Paleozoic; Paleoproterozoic. (B) Multidimensional scaling (MDS) plot (dimensionless space) for all Dahonggou and Huaitoutala detrital zircon samples, generated following methods outlined by Vermeesch (2013). Solid line indicates nearest neighbor; dashed line indicates second nearest neighbor.**

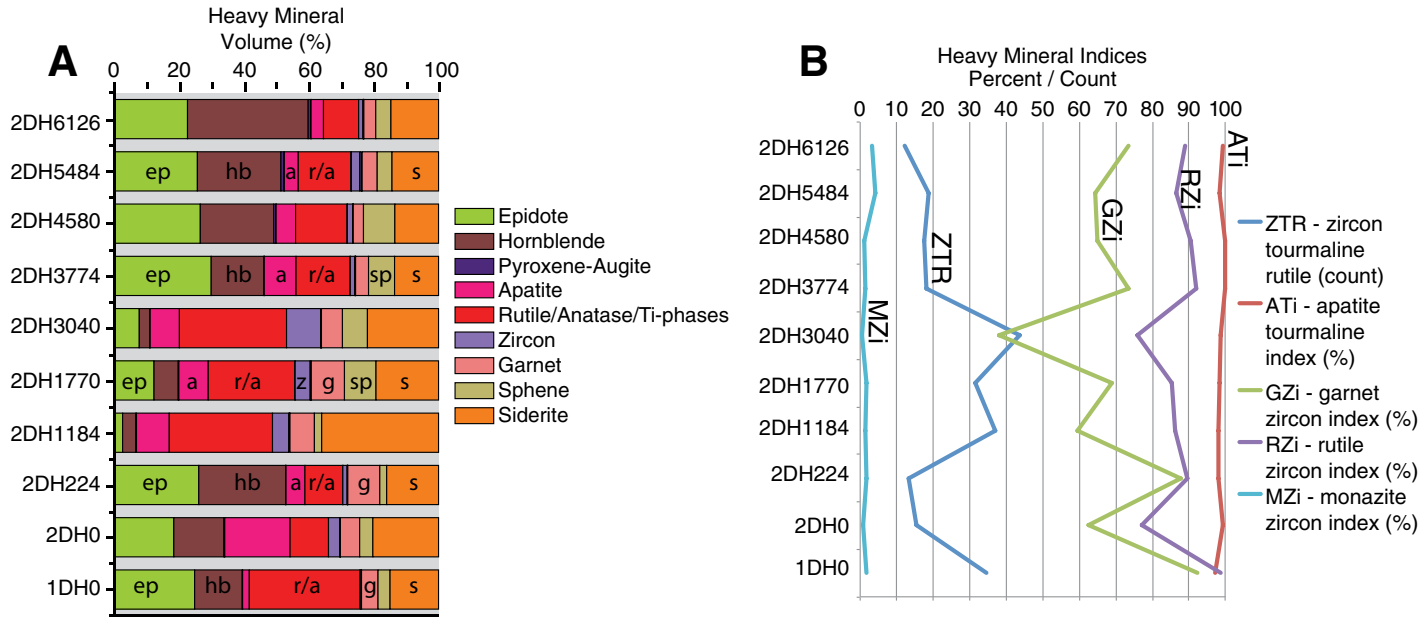


**Figure 12. Heavy mineral assemblages from Dahonggou section, plotted in stratigraphic order. (A) Heavy mineral relative abundances for heavy minerals comprising >2% of the sample. (B) Heavy mineral indices. ZTR—zircon-tourmaline-rutile index (zircon + tourmaline + rutile counts), ATi—apatite-tourmaline index [100 × apatite count/(total apatite + tourmaline)], GZi—garnet-zircon index [100 × garnet count/(total garnet + tourmaline)], RZi—$TiO_2$ group + zircon index [100 × $TiO_2$ count/(total $TiO_2$ group + zircon)], MZi—monazite-zircon index [100 × monazite count/(total monazite + zircon)].**

decreasing tourmaline (average 0.15, decreasing from 0.20 to 0.12), as well as high volumes of apatite (average 9.37), $TiO_2$ polymorphs (average 30.95), siderite (average 25.67), zircon (average 6.75), monazite (average 0.07), and sphene (average 6.54). This interval has the highest mean ZTR index (37.36), and lowest mean GZi (55.46), RZi (82.39), and MZi (1.20). Zircon, apatite, and sphene are all associated with igneous rocks, and the decrease in epidote and hornblende suggests either dilution or increasing removal of the low-grade metamorphic source. High ZTR indices characteristic of these samples are associated with enhanced recycling (Hubert, 1962).

Upper Xiaganchaigou and lower Shangganchaigou samples (2DH3040 and 2DH3774) have the highest volumes of hornblende (average 25.40), epidote (average 26.38), clinopyroxene (average 0.65), orthopyroxene (average 0.21), sphene (average 6.71), and andalusite/kyanite/sillimanite (average 0.02), yet they have the lowest volumes of apatite (average 0.03), $TiO_2$ polymorphs (average 14.90), and tourmaline (average 0.03). The lowest ZTR index (16.69) and highest ATi, RZi, and MZi are in this zone. The high abundance of metamorphic minerals (hornblende, epidote, pyroxene, andalusite/kyanite/sillimanite), low abundance of typically magmatic minerals (apatite, tourmaline), and high indices correspond to a shift from igneous (2DH1184, 2DH1770, and 2DH3040) to low- to high-grade metamorphic sources (2DH3774, 2DH4580, 2DH5484, and 2DH6126).

## Provenance Interpretations

We identified four shifts in sediment provenance based on major changes in paleocurrent orientation, heavy mineral compositions, and detrital zircon age spectra. Consistent with previous research, changes in sandstone framework grain composition at Dahonggou are minor and provide secondary constraints on provenance reconstructions (Rieser et al., 2005). The first shift involves a change from an early Paleozoic and Permian–Triassic zircon U-Pb assemblage to a largely unimodal early Paleozoic assemblage (Figs. 11A and 11B) above 220 m in the Lulehe Formation. The second shift occurs between 770 m and 1100 m in the Lulehe Formation and is characterized by a change in all three major proxies. At 770 m, paleoflow changes from eastward to southwest-directed flow (Fig. 6). At ~1100 m, there is a shift in U-Pb age spectra from an early Paleozoic assemblage to a cosmopolitan assemblage (Figs. 11A and 11B), and the heavy mineral assemblage shifts toward higher ZTR and lower GZi indices (Fig. 12). This shift is also accompanied by a minor increase in abundance of lithic grains in sandstone (Fig. 10). Between 3040 m and 3774 m, there is a return to a single early Paleozoic–dominated zircon U-Pb age spectrum coupled with a decrease in ZTR and GZi indices in the upper Xiaganchaigou–lower Shangganchaigou Formations. There is also a return to more compositionally mature sandstones. Finally, the cosmopolitan zircon U-Pb age assemblage reemerges between 4580 m and 5484 m (uppermost Shangganchaigou Formation–lower Xiayoushashan Formation) in the Dahonggou section and synchronously dominates all samples in the Huaitoutala section (Fig. 11A).

E-directed paleocurrent orientations in the lower Lulehe Formation indicate sediment sources to the south or west of the Dahonggou location. Potential sources include (1) the Hoh Xil Basin, (2) Altyn Shan, (3) Western Kunlun Shan, and (4) Eastern Kunlun Shan.

(1) Detrital zircon age spectra (1DH0 and 2DH0) lack the large Neoproterozoic, Paleoproterozoic, and Cretaceous populations of contemporaneous Lhasa-Qiangtang—derived deposits in the Hoh Xil Basin to the south (Fig. 5; Dai et al., 2012; Staisch et al., 2014), suggesting the Paleogene appearance of a Kunlun Shan topographic barrier between the Qaidam and Hoh Xil Basins.

(2) Initial displacement on the Altyn Tagh fault and uplift of the Altyn Shan are usually ascribed to Oligocene–early Miocene time, with possible Mesozoic–early Cenozoic precursor faulting (Jolivet et al., 2001; Sobel et al., 2001; Yin et al., 2002, 2007a; Cowgill et al., 2003; Darby et al., 2005; Wang et al., 2005;

Ritts et al., 2008). Because the Altyn Shan contains a major 1800–2000 Ma source (Yue et al., 2005; Gehrels et al., 2003a, 2003b) that is not observed in lower Lulehe results, it is eliminated as a possible source.

(3) On the basis of basin architecture and apatite fission-track data, Wang et al. (2006) interpreted an ~2000 km "paleo–Kunlun River" sourced in the Western Kunlun Shan to northeastern Pamir, following the incipient Altyn Tagh and Karakash faults. The expected provenance signature, however, would include early Paleozoic and Cretaceous zircons but would be dominated by Permian–Late Triassic ages (Fig. 5E; Cowgill et al., 2003; Zhang et al., 2007; Robinson et al., 2012; Carrapa et al., 2014). This association of ages is inconsistent with basal Lulehe results, which are dominated by early Paleozoic–aged zircons and include no Cretaceous ages (Fig. 11). However, exclusion of the Cretaceous-aged population would make the Western Kunlun Shan a viable secondary sediment source.

(4) Permian–Triassic and early Paleozoic age signatures from the lower Lulehe Formation (1DH0 and 2DH0) are compatible with the Kunlun arc terrane of the Eastern Kunlun Shan (west of Golmud) and southern Altyn Shan (Cowgill et al., 2003) and Triassic sedimentary units of the Kunlun Shan (Ding et al., 2013), and they are incompatible with Late Triassic plutons of the easternmost Eastern Kunlun Shan (Mo et al., 2007). The high abundance of epidote, hornblende, tourmaline, and garnet is consistent with a metamorphic basement source. Whereas low-temperature thermochronologic results from the easternmost Eastern Kunlun Shan support Oligocene–Miocene cooling (Mock et al., 1999; Jolivet et al., 2003; Yuan et al., 2006), this exhumation may be related to S-directed backthrusting following earlier Paleocene–Eocene N-directed thrusting in the Eastern Kunlun Shan (e.g., Yin et al., 2007a). Therefore, the westernmost Eastern Kunlun Shan is favored as the principal sediment source.

The switch to an early Paleozoic detrital zircon signature above 220 m occurs in the absence of a change in paleocurrent orientation, suggesting consistent derivation from the southern Qaidam Basin margin. The unimodal early Paleozoic zircon U-Pb age spectrum is consistent with a westward shift in active exhumation to the northwestern Qimen Tagh region of the Eastern Kunlun Shan, adjacent to the Altyn Shan (W. Li et al., 2013) feeding the E-directed axial fluvial system.

There is a clear switch from variable axial paleocurrents of the lower–middle Lulehe Formation to SW-directed, transverse paleocurrents at 770 m in the uppermost Lulehe and Xiaganchaigou Formations (Fig. 6). At the Dahonggou section, this interval is characterized by a cosmopolitan detrital zircon signature with Permian–Triassic, early Paleozoic, and Proterozoic age peaks. Samples from the Xiaganchaigou Formation (2DH1184, 2DH1770, 2DH3040) include Paleozoic and Paleoproterozoic grains matching the Qilian Shan–Nan Shan basement (Fig. 5; Cowgill et al., 2003; Gehrels et al., 2003a, 2003b; Menold, 2006; Yan et al., 2010). The origin of Permian–Triassic grains is more complex, because such plutons are less common in the Qilian Shan–Nan Shan than the Eastern Kunlun Shan. Given SW-directed paleocurrents and high ZTR heavy mineral index, the Permian–Triassic peak is attributed to grains recycled from Jurassic deposits situated to the north in the Qilian Shan–Nan Shan, but originally shed from the Permian–Triassic Kunlun arc (Fig. 5). The heavy mineral assemblage represents dominantly igneous and recycled sedimentary sources, consistent with populations in the Qilian Shan–Nan Shan, where a well-established catchment eroded diverse source rocks. The absence of a significant metamorphic component, common in the North Qaidam terrane, suggests that high topography was confined to the northern Qilian Shan during Xiaganchaigou deposition.

A pronounced 400–500 Ma detrital zircon age peak and corresponding reduction or disappearance of other age peaks in the two Shanganchaigou Formation samples (2DH3774, 2DH4580) could be explained by several mechanisms. First, units containing recycled Permian–Triassic and Paleoproterozoic grains may have been preferentially eroded away, leaving only lower Paleozoic rocks. Second, new drainage networks may have contained local Paleozoic sources, before drainage expansion and elaboration provided more diverse populations. Neither option, however, is likely to have completely removed two source populations while maintaining early Paleozoic sources. A third explanation involves in-sequence deformation and growth of a topographic barrier along the Nan Shan–North Qaidam thrust belt (NQF in Fig. 1). At the same level, the increase in epidote and hornblende abundance and switch to high GZi and RZi heavy mineral indices require deeper unroofing and/or exposures of metamorphic rocks. Paleoflow was to the southwest, consistent with a north/northeast source in the Qilian Shan. Possible sources include ophiolitic and ultrahigh-pressure metamorphic assemblages in the Nan Shan–North Qaidam thrust belt along the Luliang and Xitieshan thrusts (Yin et al., 2008a), or possibly farther north in the Qilian Shan–Nan Shan.

Detrital zircon ages for the uppermost Xiayoushashan–Shizigou Formations at both sections contain three major populations, including the early Paleozoic and reintroduction of Permian–Triassic and Proterozoic populations (Fig. 11). Metamorphic minerals continue to dominate heavy mineral assemblages. Lithofacies, sedimentation rates, and provenance shifts indicate continued in-sequence advance of the Luliang-Xitieshan thrust system along the southern front of the Qilian Shan–Nan Shan. Age populations can be traced to the southern Qilian Shan–Nan Shan by erosional unroofing of Paleoproterozoic basement, lower Paleozoic magmatic rocks, isolated Permian–Triassic plutons related to the Kunlun arc, as well as Mesozoic sedimentary units, collectively resulting in well-mixed detrital zircon age spectra.

## DISCUSSION

### Basin Reconstruction

Sedimentologic, provenance, and geochronologic data support a reconstruction of Qaidam Basin evolution (Fig. 13) involving multiple source regions and variations in drainage patterns dictated by shifts in the tectonic development of flanking mountain ranges. Results presented here document the Cenozoic depositional record in the northeastern Qaidam Basin, and its relation to the broader northern Tibetan Plateau. For this reconstruction, the chronology of the Dahonggou section is roughly correlated to nearby magnetostratigraphic sections (e.g., Lu and Xiong, 2009; Ke et al., 2013).

#### *Lulehe Formation (Paleocene)*

The composition and sediment dispersal pathways of Paleocene Lulehe Formation sediments are consistent with derivation from the westernmost Eastern Kunlun Shan (Fig. 2). This observation suggests that the Eastern Kunlun Shan had developed into a topographic edifice, largely or totally blocking drainage from the south (Fig. 13A). The drainage divide would have shed Permian–Triassic and early Paleozoic detritus to both the Qaidam and Hoh Xil Basins, and blocked the majority of Neoproterozoic detritus from the Qiangtang and other southern terranes (Fig. 5). Detrital zircon U-Pb data and carbonate rock fragments in the Lulehe Formation in western Qaidam confirm early exhumation of the Eastern Kunlun Shan (Cheng et al., 2015). Finally, E- and NE-directed paleocurrent orientations at the Dahonggou location on the northern margin of the Qaidam Basin also strongly suggest that the Qilian Shan was not a significant topographic barrier in the Paleocene.

#### *Lulehe Formation (Paleocene–Eocene Transition)*

The increased fluvial competence indicated by the upward-coarsening trend may be attributed to increased precipitation and runoff

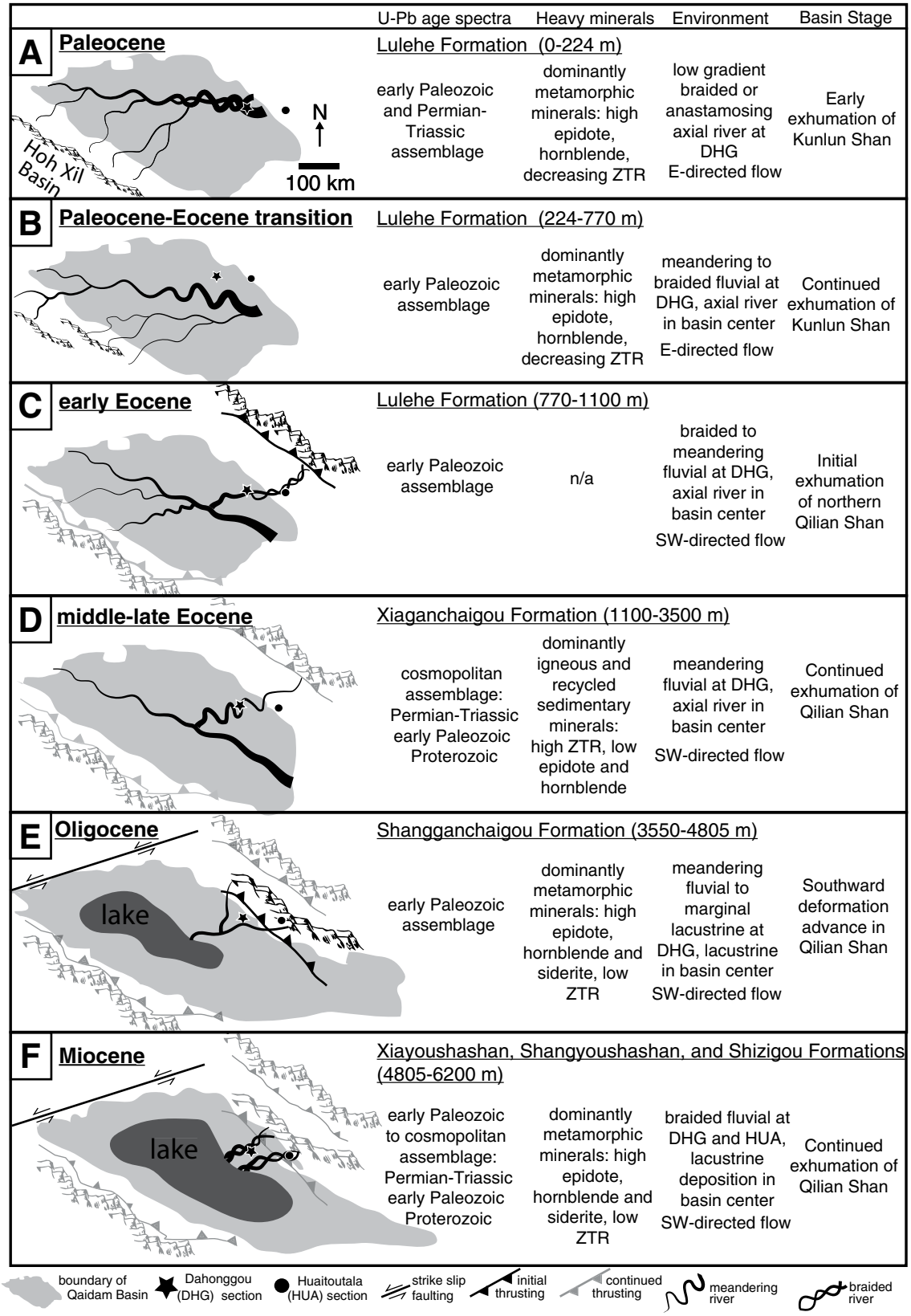


**Figure 13. Schematic diagrams of the Cenozoic Qaidam Basin evolution. Shaded basin areas are from Yin et al. (2008b) isopach maps. (A) Paleocene. (B) Paleocene-Eocene transition. (C) Early Eocene. (D) Middle–late Eocene. (E) Oligocene. (F) Miocene. Locations of sections are shown with black star (Dahonggou) and black circle (Huaitoutala). Black fault and mountain symbols show initial deformation; gray fault and mountain symbols show continued deformation and unroofing.**

or to enlargement of the catchment (Fig. 13B). However, the shift to a unimodal early Paleozoic detrital zircon peak in samples 2DH224 and 220611-01 (Fig. 11) is inconsistent with enlargement of the fluvial catchment. Oxygen isotopic values from sedimentary cements and paleosol carbonates from around the Qaidam Basin decrease from the lower to upper Lulehe Formation (Kent-Corson et al., 2009), consistent with enhanced precipitation in the late Paleocene–early Eocene. Low ZTR indices through this interval (Fig. 12), despite enhanced weathering in the warm Paleocene–Eocene climate, suggest rapid denudation and sediment transport to the Dahonggou site consistent with the increased grain size and bed-load proportions. Continued E-oriented paleoflow during this interval suggests quiescence in the Qilian Shan, continued sourcing of sediment from the SW-W basin margin, and a Qaidam Basin that remained open during this time interval.

#### *Uppermost Lulehe–Xiaganchaigou Formations (Early–Late Eocene)*

Evidence for Eocene shortening in the Qilian Shan–Nan Shan (Figs. 13C and 13D) is revealed in the Dahonggou section by shifts in lithofacies and sediment dispersal. Results indicate Eocene establishment of the northern basin margin along the southern Qilian Shan–Nan Shan north of Daqaidam (Fig. 1), with the transition to the cosmopolitan zircon assemblage at sample DH1184. Provenance data presented here are complementary to the stratigraphic synthesis of Zhuang et al. (2011), in which they recognized Eocene accumulation of coarse sediment along the southern front of the Qilian Shan and Nan Shan–North Qaidam fold-thrust belt.

#### *Shangganchaigou Formation (Oligocene)*

The transition to a dominant early Paleozoic peak during the Oligocene–early Miocene with continued SW-directed paleoflow of a meandering fluvial system requires the southward advance of the Nan Shan–North Qaidam thrust belt within the Qilian Shan (Fig. 13E). This predicts isolation from earlier sources and a huge early Paleozoic signal from plutons along the Qilian Shan–Nan Shan thrust front. A feature consistent with this interpretation is the drastic shift in heavy minerals, from a recycled sedimentary to metamorphic source. The Nan Shan–North Qaidam thrust belt contains an early Paleozoic suture zone (Mattinson et al., 2007; Xiao et al., 2009) that underwent high- and ultrahigh-pressure metamorphism, and that is exposed along the Luliang and Xitie Shan faults (Fig. 4; Yang et al., 2001; Yin et al., 2008a; Menold et al., 2009).

The Qaidam Basin was fully closed at this stage, with organic-rich lacustrine deposits accumulating in the basin center (Hanson et al., 2001). At the Dahonggou site, marginal lacustrine deposits are interbedded with paleosols and meandering fluvial deposits throughout this interval, as the depocenter shifted to the southeast due to flexural loading by the Nan Shan–North Qaidam thrust belt (Yin et al., 2008a, 2008b).

#### *Xiayoushashan, Shangyoushashan, and Shizigou Formations (Miocene–Pliocene)*

During Miocene deposition of the Xiayoushashan and Shangyoushashan Formations, the Qaidam depocenter shifted eastward (Wang et al., 2006); the deposits begin coarsening upward at the 4800 m level in the Dahonggou section, and sedimentation initiated at the Huaitoutala section (Fang et al., 2007) in a piggyback hanging-wall setting on the S-directed Luliang and Xitieshan thrust system (Fig. 13F).

Growth strata, regional unconformities, and shifts in depositional systems and accumulation rates support a deformation phase commencing at 12–8 Ma and accelerating after ca. 3.6 Ma (Clark et al., 2010; Zheng et al., 2010; Lease et al., 2011; Yuan et al., 2013). This reorganization includes diminished slip along the Altyn Tagh fault and deformation migration in the southern Qilian Shan–Nan Shan to the south and east with the development of the Eastern Luliang, Xitie Shan, and Lenghu thrusts (Yue et al., 2005; Yin et al., 2008a). In the northwestern Qaidam Basin, a shift from magmatic to metamorphic sources (Jian et al., 2013) is attributed to unroofing of the Nan Shan–North Qaidam and South Qilian Shan belts. At the Dahonggou section, diverse detrital zircon and heavy mineral assemblages imply drainage integration and source unroofing, producing diverse grains from Paleoproterozoic basement, lower Paleozoic magmatic rocks, and Permian–Triassic grains from recycled sedimentary, igneous, and metamorphic sources.

Miocene and younger deposits preserve >2000 m of coarse-grained fill, with an upward-coarsening and upward-thickening pattern reflecting progradation of large distributive fluvial lobes from range-front outlets. This succession is suggestive of the large area (>1000 km$^2$), low slope, and waterlain facies of fluvial megafans (Gupta, 1997; Horton and DeCelles, 2001; Hartley et al., 2010). During middle Miocene reorganization of deformation, a basinwide grain-size increase and initiation of deposition in the Delingha depression (subbasin containing the Huaitoutala section) represent significant topographic growth in surrounding ranges.

Modern drainage configuration and source areas were established during late Miocene–Pliocene deposition of the Shangyoushashan and Shizigou Formations (Pullen et al., 2011). Coarse-grained sediment accumulation and growth strata formation continue to characterize the modern margins and interior of the Qaidam Basin (Wang and Coward, 1990).

### Regional Implications

#### *Basin Isolation*

The pattern of basin isolation for the Qaidam region (Fig. 13) is consistent with models for plateau expansion involving structural incorporation and partitioning of once-giant peripheral basins (Métivier et al., 1998; Meyer et al., 1998; Tapponnier et al., 2001; Horton et al., 2004; Carroll et al., 2010; Craddock et al., 2011b; Horton, 2012). In this model, growth of new basin-bounding ranges forms critical topographic barriers to surface flow and atmospheric circulation, promoting sediment ponding and arid rain-shadow conditions within the basin (Sobel et al., 2003; Strecker et al., 2007). Following surface uplift, basin-margin topographic barriers and associated arid conditions inhibit erosional evacuation. Progressive partitioning of large intraplate basins is supported by studies suggesting a shared Mesozoic history for the northwestern Qaidam Basin and the southeastern Tarim Basin (Ritts and Biffi, 2000, 2001; Meng and Fang, 2008; Craddock et al., 2011a; Johnson and Ritts, 2012). Tectonic subsidence waned in the Early Cretaceous and was followed by regional burial (Jolivet et al., 2001) and potential formation of a giant peripheral basin on the northern margin of the Tibetan Plateau. The sedimentary record presented here indicates that the early Cenozoic Kunlun Shan largely isolated the Hoh Xil and Qaidam Basins by the Paleocene and would have constituted the southern margin of a formerly unified Qaidam-Tarim Basin (Ritts and Biffi, 2000; Figs. 13A and 13B).

Partitioning of this giant basin and progressive isolation of the Qaidam Basin from the Tarim Basin (to the WNW) and the Hexi Corridor (to the NE) began in the Paleogene. Paleocene to early Eocene isolation from the Hexi Corridor is documented by the provenance shift and SW-directed paleoflow in the uppermost Lulehe Formation, and displacement along thrusts bounding the NE margin of the Qaidam Basin (Fig. 13C; Yin et al., 2008a). Late Eocene–early Oligocene isolation from the Tarim Basin via movement on the Altyn Tagh fault is documented by thermochronology and basin paleogeography for the NW Qaidam region (e.g., Yue et al., 2004, 2005; Wang et al., 2005; Meng and Fang, 2008; Ritts et al., 2008). By the middle Oligocene, the Qaidam Basin was tectonically isolated from basins to the north and west. SW-directed paleoflow at Dahonggou and endorheic lacustrine deposition in western Qaidam Basin (Hanson et al., 2001) indicate that

by the Oligocene, the Qaidam Basin was also hydrologically closed. Southward encroachment of Qilian Shan fold-thrust deformation into the Qaidam Basin focused sedimentation in transverse fluvial systems along basin margins (Figs. 13C–13E). Connections to basins of the northeastern Tibetan Plateau are less clear. Increased exhumation is not documented in the Dulan-Chaka highland E of Qaidam Basin until the early Miocene (Duvall et al., 2013), raising the possibility that the Qaidam Basin remained tectonically integrated with regions to the east until at least the early Miocene.

The early Eocene onset of basin isolation is consistent with previous research suggesting that strain from India-Asia collision was transmitted rapidly to the northern edge of the modern Tibetan Plateau (e.g., Horton et al., 2004; Dupont-Nivet et al., 2004; Yin et al., 2008a; Clark et al., 2010). This may have been facilitated by high topography in the southern Tibetan Plateau (Ding et al., 2014), strong lithospheric blocks underlying the Qaidam-Tarim Basin (Braitenberg et al., 2003), and preexisting zones of weakened lithosphere in basin-bounding mountain ranges due to pre-Cenozoic deformation (Ritts and Biffi, 2001; Wang et al., 2005; Johnson and Ritts, 2012). Oxygen isotopic data from basins in the vicinity of Qaidam Basin indicate topographic growth from Eocene to Oligocene, coincident with the timing of basin isolation (Graham et al., 2005; Kent-Corson et al., 2009). Surface uplift of Qaidam Basin and its bounding ranges may have stopped or slowed due to a potential early–middle Miocene shift from largely N-S shortening to a deformation regime dominated by eastward translation of crustal blocks along continental-scale strike-slip faults (Zhang et al., 2004; Gan et al., 2007; Duvall and Clark, 2010; Zheng et al., 2010; Lease et al., 2011; Yuan et al., 2013).

### *Factors Favoring Development of Giant Basins*

The Qaidam Basin contrasts with basins in the southern Tibetan Plateau, as well as the mosaic of basins to its east in the northeastern Tibetan Plateau. Middle Miocene–Quaternary basins in the southern and central Tibetan Plateau are commonly related to extension or strike-slip faulting (e.g., Garzione et al., 2003; Spurlin et al., 2005; Kapp et al., 2008; Saylor et al., 2010; Sanchez et al., 2010; Horton, 2012; Taylor et al., 2012; Woodruff et al., 2013). Older basins in central Tibet such as Lunpola, Nima, Linzhou, and Hoh Xil (Fig. 1) formed in response to, or coeval with, shortening, and often contain only an early Cenozoic record of sedimentation, after which they were exhumed during ongoing deformation (Xu, 1984; Leeder et al., 1988; Harrison et al., 1992; Liu and Wang, 2001; Liu et al., 2001; Horton et al., 2002; DeCelles et al., 2007; He et al., 2007; Kapp et al., 2007). However, the southern and central Tibetan basins are considerably smaller, thinner, and have shorter life spans than the Qaidam Basin. Similarly, a collection of subbasins in the northeastern Tibetan Plateau have thinner stratigraphic sequences and discontinuous sedimentation, reflecting late Eocene to late Miocene segregation events (Horton et al., 2004; Dupont-Nivet et al., 2008; Lease et al., 2011), and ultimately drainage integration and evacuation in the Pleistocene (Li et al., 1997; Fang et al., 2005; Craddock et al., 2010; Nie et al., 2015).

The Qaidam region shares elements with other large basins on the periphery of the Tibetan Plateau, including the Tarim, Sichuan, and Hexi Corridor regions (Fig. 1), but it also differs from them in several fundamental ways. The Qaidam and Tarim Basins preserve the thickest and most complete Cenozoic sedimentary sequence of any of these basins, with up to 15 km of Cenozoic sediment accumulation. In the Hexi Corridor, 2.5–5 km of sediment accumulated in a restricted broken foreland basin above the basal Cretaceous–Oligocene unconformity (Bovet et al., 2009, and references therein). The Sichuan Basin contains thick sequences of Mesozoic strata, but only a thin (<1 km) veneer of Cenozoic deposits (e.g., Guo et al., 1996; Meng et al., 2005).

High-elevation basins of the southern and central Tibetan Plateau and those on the periphery are also distinguished by the strength of their crustal basement relative to that of the surrounding mountain ranges, and development of syndepositional structural dams suggesting that these factors may control their evolution and accumulation histories. Low effective elastic thicknesses (typically <20 km) of basement underlying basins in the southern and central Tibetan Plateau (Masek et al., 1994; Braitenberg et al., 2003; Jordan and Watts, 2005), and a weak layer in the middle crust–upper mantle (Jin et al., 1994; Owens and Zandt, 1997; Klemperer, 2006) allow limited evolution of overlying basins before basins are disrupted and recycled (e.g., Kapp et al., 2008). The northeastern Tibetan region is characterized by lithosphere with moderately higher but laterally heterogeneous effective elastic thickness (Braitenberg et al., 2003; Jordan and Watts, 2005; L. Li et al., 2013), resulting in strain focusing in zones of weakness, disruption of once-contiguous basins during ongoing deformation, and development of the mosaic of basins. The Hexi Corridor is characterized by ~20–30 km effective elastic thicknesses, but it is separated from the Qaidam Basin to the south by a low (<10 km) effective elastic thickness zone in the Qilian Shan–Nan Shan.

The Qaidam, Tarim, and Sichuan Basins are characterized by large regions with high effective elastic thicknesses, and high basement seismic velocities extending through the lithosphere (Braitenberg et al., 2003; Jordan and Watts, 2005; Liang and Song, 2006; Li et al., 2008a, 2008b; Li et al., 2012; Yang et al., 2012). Whereas the Tarim and Qaidam Basins developed thick Cenozoic sedimentary sequences by ponding due to Cenozoic deformation focused on the basin margins, no similar syndepositional structural dam developed in the Sichuan Basin, resulting in widespread erosion of basin strata (Richardson et al., 2008). The onset of isolation and uplift of the Qaidam Basin relative to the Tarim Basin may have been due either to injection of Tibetan lower crust beneath the Qaidam Basin (Yin et al., 2007a; Karplus et al., 2011) or structural transformation of the Qaidam Basin into a crustal-scale piggyback basin (Yin et al., 2007a; Horton, 2012).

### *Effect of Climate on Basin Filling and Evacuation*

Finally, late Eocene–early Oligocene isolation of the Qaidam Basin predates a regional increase in aridity starting in the early–middle Miocene (Kent-Corson et al., 2009; Miao et al., 2011). Endorheic conditions in Qaidam Basin also predate the increase in aridity and persist through the modern era. This sequence of events points to early defeat of range-traversing rivers by tectonic uplift and development of rain-shadow–related aridity within an isolated Qaidam Basin prior to Miocene regional aridification. On the other hand, Cenozoic strata in the multiple subbasins of northeastern Tibet point to periods of both sediment accumulation and large-scale evacuation of basin fill following regional aridification (e.g., Fang et al., 2003; Craddock et al., 2010, 2011b; Hough et al., 2011, 2014). As in the Qaidam Basin, local rain-shadow aridity is superimposed on the regional signal of aridification (Hough et al., 2014). However, excavation of the subbasins following regional aridification indicates that despite increased regional aridity in the late Cenozoic, rivers maintained sufficient stream power to overcome structurally produced topographic barriers and effectively evacuate sediments that ponded upstream of those topographic barriers. The decoupling of regional climate changes and sediment accumulation or evacuation implies that regional climate change was not the primary factor in either the development or destruction of giant plateau-margin basins.

## CONCLUSIONS

Constraints on the evolution of the Qaidam Basin provide insights into the Cenozoic de-

formation history of the northern Tibetan Plateau, which broadly include Paleocene–Eocene exhumation of the Kunlun Shan followed by activation and then outward growth of the Qilian Shan–Nan Shan. Supporting evidence consists of distinctive patterns and temporal shifts in depositional systems, detrital provenance, and sediment dispersal in the northeastern Qaidam Basin.

(1) Initial Cenozoic sedimentation in the northeastern Qaidam Basin involved eastward transport of sediment likely derived from the westernmost Eastern Kunlun Shan. Paleocene deposits (lower Lulehe Formation) contain major Permian–Triassic and early Paleozoic detrital zircon populations, with a heavy mineral assemblage of principally metamorphic origin, consistent with the Paleozoic basement, Permian–Triassic magmatic arc, and older metamorphic signatures along the Kunlun suture. These U-Pb detrital zircon ages support the existence of a drainage divide between the Qaidam Basin and the Hoh Xil Basin, preventing large volumes of Neoproterozoic grains of the Qiangtang terrane from reaching the Qaidam Basin. In the upper Lulehe Formation, a shift from sandstone- to conglomerate-dominated facies and a transition to early Paleozoic U-Pb detrital zircon ages indicate continued exhumation of the Eastern Kunlun Shan.

(2) The late Paleocene–Eocene shift is followed by an early Eocene switch to SW-directed paleoflow, igneous and recycled sedimentary heavy mineral assemblage, and diverse Permian–Triassic, early Paleozoic, and Proterozoic detrital zircon populations. This provenance analysis is consistent with the onset of extensive exhumation in the Qilian Shan–Nan Shan.

(3) In-sequence advance of the Qilian Shan–Nan Shan fold-thrust belt occurred during the Oligocene–early Miocene, with exhumation of metamorphic and ophiolitic complexes along the frontal Eastern Luliang, Xitie Shan, and Lenghu thrust faults and initial sedimentation at the Huaitoutala section located in the hanging wall of this frontal thrust belt. The Oligocene Shangganchaigou Formation preserves a significant provenance shift at the Dahonggou section, to a metamorphic heavy mineral assemblage and a unimodal early Paleozoic detrital zircon U-Pb peak.

(4) Since the middle Miocene, exhumation of the Qilian Shan–Nan Shan is recognizable in the detrital record preserved within the Qaidam Basin. Provenance data from both the Dahonggou and Huaitoutala sections show unroofing of Permian–Triassic, lower Paleozoic, and Paleoproterozoic sources, with metamorphic heavy mineral assemblages, in the Qilian Shan–Nan Shan through the Xiayoushashan and Shangyoushashan Formations, continuing through the Pliocene Shizigou Formation.

(5) During the Paleogene, the Qaidam Basin was sequentially isolated from the south, the west, and finally the north, becoming hydrologically closed by the Oligocene. The basin was eventually uplifted as a part of the Tibetan Plateau and further isolated from the basins of the northeastern Tibetan Plateau. This pattern of basin isolation and subsequent uplift demonstrates the critical role of basin formation and filling as a component in the growth of the Tibetan Plateau.

(6) This research joins a growing number of studies demonstrating the utility of an integrated approach to sediment provenance and quantitative comparison of detrital geochronology data. This is particularly true in regions where multiple sources have similar lithologies, compositions, or thermal histories or where recycling extensively masks provenance signals.

## ACKNOWLEDGMENTS

This research was supported by the University of Texas at Austin Jackson School of the Geosciences Ronald K. DeFord Field Scholarship, the American Association of Petroleum Geologists L. Austin Weeks Memorial Grant, a Geological Society of America graduate student grant, and an International Association of Sedimentologists Post-Graduate Grant Scheme awarded to Bush, and a subaward to Saylor and Horton from the National Science Foundation (NSF) grant EAR-0958704, awarded to Xiaoming Wang. Field work was facilitated by awards to Nie from the National Basic Research Program of China (grant 2013CB956400) and National Natural Science Foundation of China (grant 41422204) and logistical assistance from Yunfa Miao, Kuang He, Wenbin Peng, and Shunchuan Ji of Lanzhou University. We thank the staff at the Arizona LaserChron Center (NSF grant EAR-1032156) and Katharina Pfaff at the Colorado School of Mines QEMSCAN facility for laboratory assistance. The manuscript was improved by careful reviews by William Craddock, an anonymous reviewer, and editor Arlo Weil.

## REFERENCES CITED

Bally, A.W., Chou, I.-M., Clayton, R., Eugster, H.P., Kidwell, S., Meckel, L.D., Ryder, R.T., Watts, A.B., and Wilson, A.A., 1986, Notes on Sedimentary Basins in China: Report of the American Sedimentary Basins Delegation to the People's Republic of China Open-File Report 86, 327 p.

Bershaw, J., Garzione, C.N., Schoenbohm, L., Gehrels, G., and Tao, L., 2012, Cenozoic evolution of the Pamir plateau based on stratigraphy, zircon provenance, and stable isotopes of foreland basin sediments at Oytag (Wuyitake) in the Tarim Basin (west China): Journal of Asian Earth Sciences, v. 44, p. 136–148, doi:10.1016/j.jseaes.2011.04.020.

Besly, B.M., and Fielding, C.R., 1989, Palaeosols in Westphalian coal-bearing and red-bed sequences, central and northern England: Palaeogeography, Palaeoclimatology, Palaeoecology, v. 70, no. 4, p. 303–330, doi:10.1016/0031-0182(89)90110-7.

Bovet, P.M., Ritts, B.D., Gehrels, G.E., Abbink, A.O., Darby, B., and Hourigan, J.K., 2009, Evidence of Miocene crustal shortening in the North Qilian Shan from Cenozoic stratigraphy of the western Hexi Corridor, Gansu Province, China: American Journal of Science, v. 309, p. 290–329, doi:10.2475/00.4009.02.

Braitenberg, C., Wang, Y., Fang, J., and Hsu, H.T., 2003, Spatial variations of flexure parameters over the Tibet-Qinghai Plateau: Earth and Planetary Science Letters, v. 205, p. 211–224, doi:10.1016/S0012-821X(02)01042-7.

Cant, D.J., and Walker, R.G., 1978, Fluvial processes and facies sequences in the sandy braided South Saskatchewan River, Canada: Sedimentology, v. 25, p. 625–648, doi:10.1111/j.1365-3091.1978.tb00323.x.

Carrapa, B., Shazanee Mustapha, F., Cosca, M., Gehrels, G.E., Schoenbohm, L.M., Sobel, E.R., DeCelles, P.G., Russell, J., and Goodman, P., 2014, Multisystem dating of modern river detritus from Tajikistan and China: Implications for crustal evolution and exhumation of the Pamir: Lithosphere, v. 6, no. 6, p. 443–455, doi:10.1130/L360.1.

Carroll, A.R., Graham, S.A., and Smith, M., 2010, Walled sedimentary basins of China: Basin Research, v. 22, p. 17–32, doi:10.1111/j.1365-2117.2009.00458.x.

Chen, X.-H., Gehrels, G.E., Yin, A., Li, L., and Jiang, R.-B., 2012, Paleozoic and Mesozoic basement magmatisms of eastern Qaidam Basin, Northern Qinghai-Tibet Plateau: LA-ICP-MS zircon U-Pb geochronology and its geological significance: Acta Geologica Sinica, v. 86, p. 350–369, doi:10.1111/j.1755-6724.2012.00665.x.

Cheng, F., Fu, S., Jolivet, M., Zhang, C., and Guo, Z., 2015, Source to sink relation between the Eastern Kunlun Range and the Qaidam Basin, northern Tibetan Plateau, during the Cenozoic: Geological Society of America Bulletin v. 128, no. 1, doi:10.1130/B31260.1.

Clark, M.K., and Royden, L.H., 2000, Topographic ooze: Building the eastern margin of Tibet by lower crustal flow: Geology, v. 28, p. 703–706, doi:10.1130/0091-7613(2000)28<703:TOBTEM>2.0.CO;2.

Clark, M.K., Farley, K.A., Zheng, D., Wang, Z., and Duvall, A.R., 2010, Early Cenozoic faulting of the northern Tibetan Plateau margin from apatite (U-Th)/He ages: Earth and Planetary Science Letters, v. 296, p. 78–88, doi:10.1016/j.epsl.2010.04.051.

Cowgill, E., Yin, A., Harrison, T.M., and Wang, X.-F., 2003, Reconstruction of the Altyn Tagh fault based on U-Pb geochronology: Role of back thrusts, mantle sutures, and heterogeneous crustal strength in forming the Tibetan Plateau: Journal of Geophysical Research, v. 108, no. B7, p. 2346, doi:10.1029/2002JB002080.

Craddock, W.H., Kirby, E., Harkins, N.W., Zhang, H., Shi, X., and Liu, J., 2010, Rapid fluvial incision along the Yellow River during headward basin integration: Nature Geoscience, v. 3, no. 3, p. 209–213, doi:10.1038/ngeo777.

Craddock, W.H., Kirby, E., Zhang, D., and Liu, J., 2011a, Tectonic setting of Cretaceous basins on the NE Tibetan Plateau: Insights from the Jungong basin: Basin Research, v. 24, p. 51–69, doi:10.1111/j.1365-2117.2011.00515.x.

Craddock, W.H., Kirby, E., and Zhang, H., 2011b, Late Miocene–Pliocene range growth in the interior of the northeastern Tibetan Plateau: Lithosphere, v. 3, p. 420–438, doi:10.1130/L159.1.

Dai, J., Zhao, X., Wang, C., Zhu, L., Li, Y., and Finn, D., 2012, The vast proto–Tibetan Plateau: New constraints from Paleogene Hoh Xil Basin: Gondwana Research, v. 22, p. 434–446, doi:10.1016/j.gr.2011.08.019.

Darby, B.J., Ritts, B.D., Yue, Y., and Meng, Q., 2005, Did the Altyn Tagh fault extend beyond the Tibetan Plateau?: Earth and Planetary Science Letters, v. 240, p. 425–435, doi:10.1016/j.epsl.2005.09.011.

Dayem, K.E., Molnar, P., Clark, M.K., and Houseman, G.A., 2009, Far-field lithospheric deformation in Tibet during continental collision: Tectonics, v. 28, p. 1–9, doi:10.1029/2008TC002344.

DeCelles, P., Kapp, P., Ding, L., and Gehrels, G., 2007, Late Cretaceous to middle Tertiary basin evolution in the central Tibetan Plateau: Changing environments in response to tectonic partitioning, aridification, and regional elevation gain: Geological Society of America Bulletin, v. 119, p. 654–680, doi:10.1130/B26074.1.

Dewey, J.F., Shackleton, R.M., Chengfa, C., and Yiyin, S., 1988, The tectonic evolution of the Tibetan Plateau: Philosophical Transactions of the Royal Society, ser. A, Mathematical, Physical and Engineering Sciences, v. 327, p. 379–413, doi:10.1098/rsta.1988.0135.

Dickinson, W.R., 1970, Interpreting detrital modes of greywacke and arkose: Journal of Sedimentary Petrology, v. 40, p. 695–707.

Dickinson, W.R., 1985, Interpreting provenance relations from detrital modes of sandstones, *in* Zuffa, G.G., ed., Provenance of Arenites: Dordrecht, Netherlands, Reidel Publishing Company, p. 333–361, doi:10.1007/978-94-017-2809-6_15.

Dickinson, W.R., and Suczek, C.A., 1979, Plate Tectonics and Sandstone Compositions: American Association of Petroleum Geologists Bulletin, v. 12, p. 2164–2182.

Ding, L., Yang, D., Cai, F.L., Pullen, A., Kapp, P., Gehrels, G.E., Zhang, L.Y., Zhang, Q.H., Lai, Q.Z., Yue, Y.H., and Shi, R.D., 2013, Provenance analysis of the Mesozoic Hoh-Xil-Songpan-Ganzi turbidites in northern Tibet: Implications for the tectonic evolution of the eastern Paleo-Tethys Ocean: Tectonics, v. 32, p. 34–48, doi:10.1002/tect.20013.

Ding, L., Xu, Q., Yue, Y., Wang, H., Cai, F., and Li, S., 2014, The Andean-type Gangdese Mountains: Paleoelevation record from the Paleocene–Eocene Linzhou Basin: Earth and Planetary Science Letters, v. 392, p. 250–264, doi:10.1016/j.epsl.2014.01.045.

Dupont-Nivet, G., Horton, B.K., Butler, R.F., Wang, J., Zhou, J., and Waanders, G.L., 2004, Paleogene clockwise tectonic rotation of the Xining-Lanzhou region, northeastern Tibetan Plateau: Journal of Geophysical Research, v. 109, p. B04401, doi:10.1029/2003JB002620.

Dupont-Nivet, G., Dai, S., Fang, X., Krijgsman, W., Erens, V., Reitsma, M., and Langereis, C.G., 2008, Timing and distribution of tectonic rotations in the northeastern Tibetan Plateau, *in* Burchfiel, B.C., and Wang, E., eds., Investigations into the Tectonics of the Tibetan Plateau: Geological Society of America Special Paper 444, p. 73–87, doi:10.1130/2008.2444(05).

Duvall, A.R., and Clark, M.K., 2010, Dissipation of fast strike-slip faulting within and beyond northeastern Tibet: Geology, v. 38, p. 223–226, doi:10.1130/G30711.1.

Duvall, A.R., Clark, M.K., van der Pluijm, B.A., and Li, C., 2011, Direct dating of Eocene reverse faulting in northeastern Tibet using Ar-dating of fault clays and low-temperature thermochronometry: Earth and Planetary Science Letters, v. 304, p. 520–526, doi:10.1016/j.epsl.2011.02.028.

Duvall, A.R., Clark, M.K., Kirby, E., Farley, K.A., Craddock, W.H., Li, C., and Yuan, D.-Y., 2013, Low-temperature thermochronometry along the Kunlun and Haiyuan faults, NE Tibetan Plateau: Evidence for kinematic change during late-stage orogenesis: Tectonics, v. 32, p. 1190–1211, doi:10.1002/tect.20072.

Enkelmann, E., Weislogel, A.L., Ratschbacher, L., Eide, E., Renno, A., and Wooden, J., 2007, How was the Triassic Songpan-Ganzi basin filled? A provenance study: Tectonics, v. 26, p. TC4007, doi:10.1029/2006TC002078.

Ethridge, F.G., Skelly, R.L., and Bristow, C.S., 1999, Avulsion and crevassing in the sandy, braided Niobrara River: Complex response to base-level rise and aggradation, *in* Smith, N.D., and Rogers, J., eds., Fluvial Sedimentology VI: International Association of Sedimentologists Special Publication 28, p. 179–191, doi:10.1002/9781444304213.ch14.

Fang, X., Garzione, C., Van der Voo, R., Li, J., and Fan, M., 2003, Flexural subsidence by 29 Ma on the NE edge of Tibet from the magnetostratigraphy of Linxia Basin, China: Earth and Planetary Science Letters, v. 210, p. 545–560, doi:10.1016/S0012-821X(03)00142-0.

Fang, X., Yan, M.D., van der Voo, R., Rea, D.K., Song, C.H., Pares, J.M., Gao, J.P., Nie, J.S., and Dai, S., 2005, Late Cenozoic deformation and uplift of the NE Tibetan Plateau: Evidence from high-resolution magnetostratigraphy of the Guide Basin, Qinghai Province, China: Geological Society of America Bulletin, v. 117, p. 1208–1225, doi:10.1130/B25727.1.

Fang, X., Zhang, W., Meng, Q., Gao, J., Wang, X., King, J.G., Song, C., Dai, S., and Miao, Y., 2007, High-resolution magnetostratigraphy of the Neogene Huaitoutala section in the eastern Qaidam Basin on the NE Tibetan Plateau, Qinghai Province, China, and its implication on tectonic uplift of the NE Tibetan Plateau: Earth and Planetary Science Letters, v. 258, p. 293–306, doi:10.1016/j.epsl.2007.03.042.

Fielding, C.R., 1986, Fluvial channel and overbank deposits from the Westphalian of the Durham coalfield, NE England: Sedimentology, v. 33, no. 1, p. 119–140, doi:10.1111/j.1365-3091.1986.tb00748.x.

Folk, R.L., 1980, Petrology of Sedimentary Rocks: Austin, Texas, Hemphill Publishing Company, 190 p.

Friend, P.F., Slater, M.J., and Williams, R.C., 1979, Vertical and lateral building of river sandstone bodies, Ebro Basin, Spain: Journal of the Geological Society of London, v. 136, p. 39–46, doi:10.1144/gsjgs.136.1.0039.

Fu, B., and Awata, Y., 2007, Displacement and timing of left-lateral faulting in the Kunlun fault zone, northern Tibet, inferred from geologic and geomorphic features: Journal of Asian Earth Sciences, v. 29, p. 253–265, doi:10.1016/j.jseaes.2006.03.004.

Gan, W., Zhang, P., Shen, Z.K., Niu, Z., Wang, M., Wan, Y., Zhou, D., and Cheng, J., 2007, Present-day crustal motion within the Tibetan Plateau inferred from GPS measurements: Journal of Geophysical Research, v. 112, p. B08416, doi:10.1029/2005JB004120.

Gao, J., Li, S., Dai, S., Li, A., and Peng, Y., 2009, Constraints of tectonic evolution in provenance from detrital zircon fission-track data of Cenozoic strata of Xichogou district in western Qaidam Basin: Journal of Lanzhou University (Natural Sciences), v. 45, p. 1–7.

Garzione, C., DeCelles, P., Hodkinson, D., Ojha, T., and Upreti, B., 2003, East-west extension and Miocene environmental change in the southern Tibetan Plateau: Thakkhola graben, central Nepal: Geological Society of America Bulletin, v. 115, p. 3–20, doi:10.1130/0016-7606(2003)115<0003:EWEAME>2.0.CO;2.

Gazzi, P., 1966, Le minerali pesanti nei flysch arenacei fra Monte Ramaceto e Monte Molinatico (Appennino settent Ríonale): Mineralogica et Petrographica Acta, v. 11, p. 197–212.

Gehrels, G.E., Yin, A., and Wang, X.-F., 2003a, Detrital-zircon geochronology of the northeastern Tibetan Plateau: Geological Society of America Bulletin, v. 115, p. 881–896, doi:10.1130/0016-7606(2003)115<0881:DGOTNT>2.0.CO;2.

Gehrels, G.E., Yin, A., and Wang, X.-F., 2003b, Magmatic history of the northeastern Tibetan Plateau: Journal of Geophysical Research, v. 108, no. B9, p. 1–14, doi:10.1029/2002JB001876.

Gehrels, G.E., Valencia, V.A., and Ruiz, J., 2008, Enhanced precision, accuracy, efficiency, and spatial resolution of U-Pb ages by laser ablation–multicollector–inductively coupled plasma–mass spectrometry: Geochemistry Geophysics Geosystems, v. 9, p. 1–13, doi:10.1029/2007GC001805.

Gehrels, G.E., Kapp, P., DeCelles, P.G., Pullen, A., Blakey, R., Weislogel, A.L., Ding, L., Guynn, J., Martin, A., McQuarrie, N., and Yin, A., 2011, Detrital zircon geochronology of pre-Tertiary strata in the Tibetan-Himalayan orogen: Tectonics, v. 30, p. TC5016, doi:10.1029/2011TC002868.

George, A.D., Marshallsea, S.J., Wyrwoll, K.-H., Jie, C., and Yanchou, L., 2001, Miocene cooling in the northern Qilian Shan, northeastern margin of the Tibetan Plateau, revealed by apatite fission-track and vitrinite-reflectance analysis: Geology, v. 29, p. 939–942, doi:10.1130/0091-7613(2001)029<0939:MCITNQ>2.0.CO;2.

Graham, S.A., Hendrix, M.S., Wang, L.B., and Carroll, A.R., 1993, Collisional successor basins of western China—Impact of tectonic inheritance on sand composition: Geological Society of America Bulletin, v. 105, no. 3, p. 323–344, doi:10.1130/0016-7606(1993)105<0323:CSBOWC>2.3.CO;2.

Graham, S.A., Chamberlain, C.P., Yue, Y., Ritts, B.D., Hanson, A.D., Horton, T.W., Waldbauer, J.R., Poage, M.A., and Feng, X., 2005, Stable isotope records of Cenozoic climate and topography, Tibetan Plateau and Tarim Basin: American Journal of Science, v. 305, p. 101–118, doi:10.2475/ajs.305.2.101.

Guo, Z., Deng, K., and Han, Y., 1996, Formation and Evolution of the Sichuan Basin: Beijing, Geologic Publishing House, 200 p.

Gupta, S., 1997, Himalayan drainage patterns and the origin of fluvial megafans in the Ganges foreland basin: Geology, v. 25, p. 11–14, doi:10.1130/0091-7613(1997)025<0011:HDPATO>2.3.CO;2.

Hanson, A.D., 1999, Organic geochemistry and petroleum geology, tectonics and basin analysis of southern Tarim and northern Qaidam basins, northwest China [Ph.D. thesis]: Stanford, California, Stanford University, 388 p.

Hanson, A.D., Ritts, B.D., Zinniker, D., Moldowan, J.M., and Biffi, U., 2001, Upper Oligocene lacustrine source rocks and petroleum systems of the northern Qaidam Basin, northwest China: American Association of Petroleum Geologists Bulletin, v. 85, p. 601–619.

Harris, N.B.W., Ronghua, X., Lewis, C.L., and Chengwei, J., 1988, Plutonic rocks of the 1985 Tibet Geotraverse, Lhasa to Golmud: Philosophical Transactions of the Royal Society, ser. A, Mathematical, Physical and Engineering Sciences, v. 327, p. 145–168, doi:10.1098/rsta.1988.0124.

Harrison, T., Copeland, P., Kidd, W., and Yin, A., 1992, Raising Tibet: Science, v. 255, no. 5052, p. 1663–1670, doi:10.1126/science.255.5052.1663.

Hartley, A.J., Weissmann, G.S., Nichols, G.J., and Warwick, G.L., 2010, Large distributive fluvial systems: Characteristics, distribution, and controls on development: Journal of Sedimentary Research, v. 80, p. 167–183, doi:10.2110/jsr.2010.016.

He, S.D., Kapp, P., DeCelles, P.G., Gehrels, G.E., and Heizler, M., 2007, Cretaceous–Tertiary geology of the Gangdese Arc in the Linzhou area, southern Tibet: Tectonophysics, v. 433, p. 15–37, doi:10.1016/j.tecto.2007.01.005.

Horton, B.K., 2012, Cenozoic evolution of hinterland basins in the Andes and Tibet, *in* Busby, C., and Azor, A., eds., Tectonics of Sedimentary Basins: Recent Advances: Oxford, UK, Wiley-Blackwell, p. 427–444, doi:10.1002/9781444347166.ch21.

Horton, B.K., and DeCelles, P.G., 2001, Modern and ancient fluvial megafans in the foreland basin system of the central Andes, southern Bolivia: Implications for drainage network evolution in fold-thrust belts: Basin Research, v. 13, p. 43–63, doi:10.1046/j.1365-2117.2001.00137.x.

Horton, B.K., Yin, A., Spurlin, M.S., Zhou, J.Y., and Wang, J.H., 2002, Paleocene–Eocene syncontractional sedimentation in narrow, lacustrine-dominated basins of east-central Tibet: Geological Society of America Bulletin, v. 114, p. 771–786, doi:10.1130/0016-7606(2002)114<0771:PESSIN>2.0.CO;2.

Horton, B.K., Dupont-Nivet, G., Zhou, J., Waanders, G.L., Butler, R.F., and Wang, J., 2004, Mesozoic–Cenozoic evolution of the Xining-Minhe and Dangchang basins, northeastern Tibetan Plateau: Magnetostratigraphic and biostratigraphic results: Journal of Geophysical Research, v. 109, p. B04402, doi:10.1029/2003JB002913.

Hough, B.G., Garzione, C.N., Wang, Z., Lease, R.O., Burbank, D.W., and Yuan, D., 2011, Stable isotope evidence for topographic growth and basin segmentation: Implications for the evolution of the NE Tibetan Plateau: Geological Society of America Bulletin, v. 123, p. 168–185, doi:10.1130/B30090.1.

Hough, B.G., Garzione, C.N., Wang, Z., and Lease, R.O., 2014, Timing and spatial patterns of basin segmentation and climate change in northeastern Tibet, *in* Nie, J., Horton, B.K., and Hoke, G.D., eds., Toward an Improved Understanding of Uplift Mechanisms and the Elevation History of the Tibetan Plateau: Geological Society of America Special Paper 507, p. 129–153, doi:10.1130/2014.2507(07).

Hsü, K.J., Guitang, P., and Sengör, A., 1995, Tectonic evolution of the Tibetan Plateau: A working hypothesis based on the archipelago model of orogenesis: International Geology Review, v. 37, p. 473–508, doi:10.1080/00206819509465414.

Hubert, J.F., 1962, A zircon-tourmaline-rutile maturity index and the interdependence of the composition of heavy mineral assemblages with the gross composition and texture of sandstones: Journal of Sedimentary Petrology, v. 32, p. 440–450.

Jian, X., Guan, P., Zhang, D.-W., Zhang, W., Feng, F., Liu, R.-J., and Lin, S.-D., 2013, Provenance of Tertiary sandstone in the northern Qaidam Basin, northeastern Tibetan Plateau: Integration of framework petrography, heavy mineral analysis and mineral chemistry: Sedimentary Geology, v. 290, p. 109–125, doi:10.1016/j.sedgeo.2013.03.010.

Jin, Y., McNutt, M.K., and Zhu, Y., 1994, Evidence from gravity and topography data for folding of Tibet: Nature, v. 371, no. 6499, p. 669–674, doi:10.1038/371669a0.

Johnson, C.L., and Ritts, B.D., 2012, Plate interior poly-phase basins, *in* Busby, C., and Azor, P.A., eds., Tectonics of Sedimentary Basins: Recent Advances: Oxford, UK, Wiley-Blackwell, p. 567–582, doi:10.1002/9781444347166.ch28.

Jolivet, M., Brunel, M., Seward, D., Xu, Z., Yang, J., Roger, F., Tapponnier, P., Malavieille, J., Arnaud, N., and Wu, C., 2001, Mesozoic and Cenozoic tectonics of the northern edge of the Tibetan Plateau: Fission-track constraints: Tectonophysics, v. 343, p. 111–134, doi:10.1016/S0040-1951(01)00196-2.

Jolivet, M., Brunel, M., Seward, D., Xu, Z., Yang, J., Malavieille, J., Roger, F., Leyreloup, A., Arnaud, N., and Wu, C., 2003, Neogene extension and volcanism in the Kunlun fault zone, northern Tibet: New constraints on the age

of the Kunlun fault: Tectonics, v. 22, p. 1052, doi:10.1029/2002TC001428.

Jordan, T., and Watts, A., 2005, Gravity anomalies, flexure and the elastic thickness structure of the India–Eurasia collisional system: Earth and Planetary Science Letters, v. 236, p. 732–750, doi:10.1016/j.epsl.2005.05.036.

Kapp, P., DeCelles, P.G., Gehrels, G.E., Heizier, M., and Ding, L., 2007, Geological records of the Lhasa-Qiangtang and Indo-Asian collisions in the Nima area of central Tibet: Geological Society of America Bulletin, v. 119, p. 917–933, doi:10.1130/B26033.1.

Kapp, P., Taylor, M., Stockli, D., and Ding, L., 2008, Development of active low-angle normal fault systems during orogenic collapse: Insight from Tibet: Geology, v. 36, no. 1, p. 7–10, doi:10.1130/G24054A.1.

Karplus, M., Zhao, W., Klemperer, S.L., Wu, Z., Mechie, J., Shi, D., Brown, L.D., and Chen, C., 2011, Injection of Tibetan crust beneath the south Qaidam Basin: Evidence from INDEPTH IV wide-angle seismic data: Journal of Geophysical Research, v. 116, p. 1–23, doi:10.1029/2010JB007911.

Ke, X., Ji, J., Zhang, K., Kou, X., Song, B., and Wang, C., 2013, Magnetostratigraphy and anisotropy of magnetic susceptibility of the Lulehe formation in the northeastern Qaidam basin: Acta Geologica Sinica, v. 87, p. 576–587, doi:10.1111/1755-6724.12069 [English edition].

Kent-Corson, M.L., Ritts, B.D., Zhuang, G., Bovet, P.M., Graham, S.A., and Chamberlain, P., 2009, Stable isotopic constraints on the tectonic, topographic, and climatic evolution of the northern margin of the Tibetan Plateau: Earth and Planetary Science Letters, v. 282, p. 158–166, doi:10.1016/j.epsl.2009.03.011.

Kirby, E., Harkins, N.W., Wang, E., Shi, X., Fan, C., and Burbank, D.W., 2007, Slip rate gradients along the eastern Kunlun fault: Tectonics, v. 26, p. 1–16, doi:10.1029/2006TC002033.

Klemperer, S.L., 2006, Crustal flow in Tibet: Geophysical evidence for the physical state of Tibetan lithosphere, and inferred patterns of active flow, *in* Law, R.D., Searle, M.P., and Godin, L., eds., Channel Flow, Ductile Extrusion and Exhumation in Continental Collision Zones: Geological Society of London Special Publication 268, p. 39–70, doi:10.1144/GSL.SP.2006.268.01.03.

Kraus, M., 1996, Avulsion deposits in lower Eocene alluvial rocks, Bighorn Basin, Wyoming: Journal of Sedimentary Research, v. 66, p. 354–363.

Lease, R.O., Burbank, D.W., Clark, M.K., Farley, K.A., Zheng, D., and Zhang, H., 2011, Middle Miocene reorganization of deformation along the northeastern Tibetan Plateau: Geology, v. 39, p. 359–362, doi:10.1130/G31356.1.

Leeder, M.R., Smith, A.B., and Yin, J., 1988, Sedimentology, palaeoecology and palaeoenvironmental evolution of the 1985 Lhasa to Golmud Geotraverse: Philosophical Transactions of the Royal Society of London, ser. A, Mathematical, Physical and Engineering Sciences, v. 327, p. 107–143, doi:10.1098/rsta.1988.0123.

Li, C., van der Hilst, R.D., Engdahl, E.R., and Burdick, S., 2008a, A new global model for P wave speed variations in Earth's mantle: Geochemistry Geophysics Geosystems, v. 9, doi:10.1029/2007GC001806.

Li, C., Van der Hilst, R.D., Meltzer, A.S., and Engdahl, E.R., 2008b, Subduction of the Indian lithosphere beneath the Tibetan Plateau and Burma: Earth and Planetary Science Letters, v. 274, p. 157–168, doi:10.1016/j.epsl.2008.07.016.

Li, H., Li, S., Song, X., Gong, M., Li, X., and Jia, J., 2012, Crustal and uppermost mantle velocity structure beneath northwestern China from seismic ambient noise tomography: Geophysical Journal International, v. 188, p. 131–143, doi:10.1111/j.1365-246X.2011.05205.x.

Li, J.-J., Fang, X.-M., Van der Voo, R., Zhu, J.-J., Niocaill, C.M., Ono, Y., Pan, B.-T., Zhong, W., Wang, J.-L., Sasaki, T., Zhang, Y.-T., Cao, J.-X., Kang, S.-C., and Wang, J.-M., 1997, Magnetostratigraphic dating of river terraces: Rapid and intermittent incision by the Yellow River of the northeastern margin of the Tibetan Plateau during the Quaternary: Journal of Geophysical Research–Solid Earth, v. 102, p. 10,121–10,132, doi:10.1029/97JB00275.

Li, L., Li, A., Shen, Y., Sandvol, E.A., Shi, D., Li, H., and Li, X., 2013, Shear wave structure in the northeastern Tibetan Plateau from Rayleigh wave tomography: Journal of Geophysical Research–Solid Earth, v. 118, p. 4170–4183, doi:10.1002/jgrb.50292.

Li, L., Guo, Z., Guan, S., Zhou, S., Wang, M., Fang, Y., and Zhang, C., 2015, Heavy mineral assemblage characteristics and the Cenozoic paleogeographic evolution in southwestern Qaidam Basin: Science: China Earth Sciences, v. 58, p. 859–875, doi:10.1007/s11430-014-5050-x.

Li, W., Neubauer, F., Liu, Y., Genser, J., Ren, S., Han, G., and Liang, C., 2013, Paleozoic evolution of the Qimantagh magmatic arcs, Eastern Kunlun Mountains: Constraints from zircon dating of granitoids and modern river sands: Journal of Asian Earth Sciences, v. 77, p. 183–202, doi:10.1016/j.jseaes.2013.08.030.

Liang, C., and Song, X., 2006, A low velocity belt beneath northern and eastern Tibetan Plateau from Pn tomography: Geophysical Research Letters, v. 33, p. L22306, doi:10.1029/2006GL027926.

Lin, A., Fu, B., Guo, J., Zeng, Q., Dang, G., He, W., and Zhao, Y., 2002, Co-seismic strike-slip and rupture length produced by the 2001 Ms 8.1 Central Kunlun earthquake: Science, v. 296, no. 5575, p. 2015–2017, doi:10.1126/science.1070879.

Liu, C., Mo, X., Luo, Z., Yu, X., Chen, H., Li, S., and Zhao, X., 2004, Mixing events between the crust- and mantle-derived magmas in Eastern Kunlun: Evidence from zircon SHRIMP II chronology: Chinese Science Bulletin, v. 49, p. 828–834, doi:10.1007/BF02889756.

Liu, Z.F., and Wang, C.S., 2001, Facies analysis and depositional systems of Cenozoic sediments in the Hoh Xil Basin, northern Tibet: Sedimentary Geology, v. 140, p. 251–270, doi:10.1016/S0037-0738(00)00188-3.

Liu, Z., Wang, C., and Yi, H., 2001, Evolution and mass accumulation of the Cenozoic Hoh Xil Basin, northern Tibet: Journal of Sedimentary Research, v. 71, p. 971–984, doi:10.1306/030901710971.

Lu, H., and Xiong, S., 2009, Magnetostratigraphy of the Dahonggou section, northern Qaidam Basin, and its bearing on Cenozoic tectonic evolution of the Qilian Shan and Altyn Tagh fault: Earth and Planetary Science Letters, v. 288, p. 539–550, doi:10.1016/j.epsl.2009.10.016.

Lu, H., Wang, E., Shi, X., and Meng, K., 2012, Cenozoic tectonic evolution of the Elashan range and its surroundings, northern Tibetan Plateau, as constrained by paleomagnetism and apatite fission track analyses: Tectonophysics, v. 580, p. 150–161, doi:10.1016/j.tecto.2012.09.013.

Makaske, B., 2001, Anastomosing rivers: A review of their classification, origin and sedimentary products: Earth-Science Reviews, v. 53, p. 149–196, doi:10.1016/S0012-8252(00)00038-6.

Mange, M., and Maurer, H.F.W., 1992, Heavy Minerals in Colour: Hong Kong, Chapman & Hall, doi:10.1007/978-94-011-2308-2.

Mao, L., Xiao, A., Wu, L., Li, B., Wang, L., Lou, Q., Dong, Y., and Qin, S., 2014, Cenozoic tectonic and sedimentary evolution of southern Qaidam Basin, NE Tibetan Plateau, and its implication for the rejuvenation of Eastern Kunlun Mountains: Science China—Earth Sciences, v. 57, doi:10.1007/s11430-014-4951-z.

Masek, J.G., Isacks, B.L., Fielding, E.J., and Browaeys, J., 1994, Rift flank uplift in Tibet: Evidence for a viscous lower crust: Tectonics, v. 13, p. 659–667, doi:10.1029/94TC00452.

Mattinson, C.G., Menold, C.A., Zhang, J.X., and Bird, D.K., 2007, High- and ultrahigh-pressure metamorphism in the North Qaidam and South Altyn terranes, western China: International Geology Review, v. 49, p. 969–995, doi:10.2747/0020-6814.49.11.969.

McRivette, M.W., 2011, The Tectonic Evolution of the Eastern Kunlun Range and Central Tibetan Plateau, China [Ph.D. dissertation]: Los Angeles, California, University of California, 333 p.

Meng, Q.R., and Fang, X., 2008, Cenozoic tectonic development of the Qaidam Basin in the northeastern Tibetan Plateau, *in* Burchfiel, B.C., and Wang, E., eds., Investigations into the Tectonics of the Tibetan Plateau: Geological Society of America Special Paper 444, p. 1–24, doi:10.1130/2008.2444(01).

Meng, Q.-R., Wang, E., and Hu, J.-M., 2005, Mesozoic sedimentary evolution of the northwest Sichuan Basin: Implication for continued clockwise rotation of the South China block: Geological Society of America Bulletin, v. 117, p. 396–410, doi:10.1130/B25407.1.

Menold, C.A., 2006, Tectonic and Metamorphic Evolution of the North Qaidam Ultrahigh-Pressure Metamorphic Terrane, Western China [Ph.D. dissertation]: Los Angeles, California, University of California, 279 p.

Menold, C.A., Manning, C.E., Yin, A., Tropper, P., Chen, X.-H., and Wang, X.-F., 2009, Metamorphic evolution, mineral chemistry and thermobarometry of orthogneiss hosting ultrahigh-pressure eclogites in the North Qaidam metamorphic belt, western China: Journal of Asian Earth Sciences, v. 35, p. 273–284, doi:10.1016/j.jseaes.2008.12.008.

Métivier, F., Gaudemer, Y., Tapponnier, P., and Meyer, B., 1998, Northeastward growth of the Tibet Plateau deduced from balanced reconstruction of two depositional areas: Tectonics, v. 17, p. 823–842, doi:10.1029/98TC02764.

Meyer, B., Tapponnier, P., Bourjot, L., Metivier, F., Gaudemer, Y., Peltzer, G., Shunmin, G., and Zhitai, C., 1998, Crustal thickening in Gansu-Qinghai, lithospheric mantle subduction, and oblique, strike-slip controlled growth of the Tibetan Plateau: Geophysical Journal International, v. 135, p. 1–47, doi:10.1046/j.1365-246X.1998.00567.x.

Miall, A.D., 1977, A review of the braided-river depositional environment: Earth-Science Reviews, v. 13, p. 1–62, doi:10.1016/0012-8252(77)90055-1.

Miall, A.D., 2013, The Geology of Fluvial Deposits: Heidelberg, Springer-Verlag, 582 p.

Miao, Y., Fang, X., Song, Z., Wu, F., Han, W., Dai, S., and Song, C., 2008, Late Eocene pollen records and palaeoenvironmental changes in northern Tibetan Plateau: Science in China, ser. D, Earth Science, v. 51, p. 1089–1098, doi:10.1007/s11430-008-0091-7.

Miao, Y., Fang, X., Herrmann, M., Wu, F., Zhang, Y., and Liu, D., 2011, Miocene pollen record of KC-1 core in the Qaidam Basin, NE Tibetan Plateau, and implications for evolution of the East Asian monsoon: Palaeogeography, Palaeoclimatology, Palaeoecology, v. 299, p. 30–38, doi:10.1016/j.palaeo.2010.10.026.

Mo, X., Luo, Z., Deng, J., Yu, X., Liu, C., Chen, H., Yuan, W., and Liu, Y., 2007, Granitoids and crustal growth in the East-Kunlun orogenic belt: Geological Journal of China Universities, v. 13, p. 403–414.

Mock, C., Arnaud, N.O., and Cantagrel, J.-M., 1999, An early unroofing in northeastern Tibet? Constraints from $^{40}Ar/^{39}Ar$ thermochronology on granitoids from the eastern Kunlun range: Earth and Planetary Science Letters, v. 171, p. 107–122, doi:10.1016/S0012-821X(99)00133-8.

Morton, A.C., and Hallsworth, C.R., 1994, Identifying provenance-specific features of detrital heavy mineral assemblages in sandstones: Sedimentary Geology, v. 90, p. 241–256, doi:10.1016/0037-0738(94)90041-8.

Nanson, G., 1980, Point bar and floodplain formation of the meandering Beatton River, northeastern British Columbia, Canada: Sedimentology, v. 27, p. 3–29, doi:10.1111/j.1365-3091.1980.tb01155.x.

Nemec, W., and Steel, R.J., 1984, Alluvial and coastal conglomerates: Their significance and some comments on gravelly mass-flow deposits, *in* Koster, E.H., and Steel, R.J., eds., Sedimentology of Gravels and Conglomerates: Canadian Society of Petroleum Geologists Memoir 10, p. 1–31.

Nie, J., Stevens, T., Rittner, M., Stockli, D., Garzanti, E., Limonta, M., Bird, A., Ando, S., Vermeesch, P., Saylor, J., Lu, H., Breecker, D., Hu, X., Liu, S., Resentini, A., Vezzoli, G., Peng, W., Carter, A., Ji, S., and Pan, B., 2015, Loess Plateau storage of northeastern Tibetan Plateau–derived Yellow River sediment: Nature Communications, v. 6, p. 8511, doi:10.1038/ncomms9511.

Owens, T.J., and Zandt, G., 1997, Implications of crustal property variations for models of Tibetan Plateau evolution: Nature, v. 387, no. 6628, p. 37–43, doi:10.1038/387037a0.

Porter, R.J., and Gallois, R.W., 2008, Identifying fluvio-lacustrine intervals in thick playa-lake successions: An integrated sedimentology and ichnology of arenaceous members in the mid–Late Triassic Mercia Mudstone Group of south-west England, UK: Palaeogeography, Palaeoclimatology, Palaeoecology, v. 270, p. 381–398, doi:10.1016/j.palaeo.2008.07.020.

Pullen, A., Kapp, P., Gehrels, G.E., Vervoort, J.D., and Ding, L., 2008, Triassic continental subduction in central Tibet and Mediterranean-style closure of the Paleo-Tethys Ocean: Geology, v. 36, p. 351, doi:10.1130/G24435A.1.

Pullen, A., Kapp, P., McCallister, A.T., Chang, H., Gehrels, G.E., Garzione, C.N., Heermance, R.V., and Ding, L., 2011, Qaidam Basin and northern Tibetan Plateau as dust

sources for the Chinese Loess Plateau and paleoclimatic implications: Geology, v. 39, no. 11, p. 1031-1034, doi:10.1130/G32296.1.

Qinghai Bureau of Geology and Mineral Resources, 1991, Regional Geology of Qinghai Province: Beijing, Geological Publishing House, 662 p.

Richardson, N.J., Densmore, A.L., Seward, D., Fowler, A., Wipf, M., Ellis, M.A., Yong, L., and Zhang, Y., 2008, Extraordinary denudation in the Sichuan Basin: Insights from low-temperature thermochronology adjacent to the eastern margin of the Tibetan Plateau: Journal of Geophysical Research–Solid Earth, v. 113, p. B04409, doi:10.1029/2006JB004739.

Rieser, A.B., Neubauer, F., Liu, Y., and Ge, X., 2005, Sandstone provenance of north-western sectors of the intracontinental Cenozoic Qaidam Basin, western China: Tectonic vs. climatic control: Sedimentary Geology, v. 177, p. 1–18, doi:10.1016/j.sedgeo.2005.01.012.

Rieser, A.B., Liu, Y., Genser, J., Neubauer, F., Handler, R., Friedl, G., and Ge, X., 2006a, $^{40}Ar/^{39}Ar$ ages of detrital white mica constrain the Cenozoic development of the intracontinental Qaidam Basin, China: Geological Society of America Bulletin, v. 118, p. 1522–1534, doi:10.1130/B25962.1.

Rieser, A.B., Liu, Y.J., Genser, J., Neubauer, F., Handler, R., and Ge, X.H., 2006b, Uniform Permian Ar-40/Ar-39 detrital mica ages in the eastern Qaidam Basin (NW China): Where is the source?: Terra Nova, v. 18, no. 1, p. 79–87, doi:10.1111/j.1365-3121.2005.00666.x.

Ritts, B.D., 1998, Mesozoic Tectonics and Sedimentation, and Petroleum Systems of the Qaidam and Tarim Basins, NW China [Ph.D. dissertation]: Stanford, California, Stanford University, 691 p.

Ritts, B.D., and Biffi, U., 2000, Magnitude of post–Middle Jurassic (Bajocian) displacement on the central Altyn Tagh fault system, northwest China: Geological Society of America Bulletin, v. 112, p. 61–74, doi:10.1130/0016-7606(2000)112<61:MOPJBD>2.0.CO;2.

Ritts, B.D., and Biffi, U., 2001, Mesozoic northeast Qaidam Basin: Response to contractional reactivation of the Qilian Shan, and implications for the extent of Mesozoic intracontinental deformation in Central Asia, *in* Hendrix, M.S., and Davis, G.A., eds., Paleozoic and Mesozoic Tectonic Evolution of Central and Eastern Asia: From Continental Assembly to Intracontinental Deformation: Geological Society of America Memoir 194, p. 293–316, doi:10.1130/0-8137-1194-0.293.

Ritts, B.D., Yue, Y., Graham, S.A., Sobel, E.R., Abbink, A.O., and Stockli, D.F., 2008, From sea level to high elevation in 15 million years: Uplift history of the northern Tibetan Plateau margin in the Altun Shan: American Journal of Science, v. 308, p. 657–678, doi:10.2475/05.2008.01.

Robinson, A.C., Ducea, M., and Lapen, T.J., 2012, Detrital zircon and isotopic constraints on the crustal architecture and tectonic evolution of the northeastern Pamir: Tectonics, v. 31, p. TC2016, doi:10.1029/2011TC003013.

Roger, F., Arnaud, N., Gilder, S., Tapponnier, P., Jolivet, M., Brunel, M., Malavieille, J., Xu, Z., and Yang, J., 2003, Geochronological and geochemical constraints on Mesozoic suturing in east central Tibet: Tectonics, v. 22, p. 1037, doi:10.1029/2002TC001466.

Rust, B.R., 1972, Structure and process in a braided river: Sedimentology, v. 18, p. 221–245, doi:10.1111/j.1365-3091.1972.tb00013.x.

Sanchez, V.I., Murphy, M.A., Dupré, W.R., Ding, L., and Zhang, R., 2010, Structural evolution of the Neogene Gar Basin, western Tibet: Implications for releasing bend development and drainage patterns: Geological Society of America Bulletin, v. 122, p. 926–945, doi:10.1130/B26566.1.

Saylor, J.E., DeCelles, P.C., Gehrels, G., Murphy, M., Zhang, R., and Kapp, P., 2010, Basin formation in the High Himalaya by arc-parallel extension and tectonic damming: Zhada Basin, southwestern Tibet: Tectonics, v. 29, p. TC1004, doi:10.1029/2008TC002390.

Smith, S.A., 1990, The sedimentology and accretionary styles of an ancient gravel-bed stream: The Budleigh Salterton Pebble Beds (Lower Triassic), southwest England: Sedimentary Geology, v. 67, p. 199–219, doi:10.1016/0037-0738(90)90035-R.

Sobel, E.R., and Arnaud, N., 1999, A possible middle Paleozoic suture in the Altyn Tagh, NW China: Tectonics, v. 18, p. 64–74, doi:10.1029/1998TC900023.

Sobel, E.R., Arnaud, N., Jolivet, M., and Ritts, B.D., 2001, Jurassic to Cenozoic exhumation history of the Altyn Tagh range, northwest China, constrained by $^{40}Ar/^{39}Ar$ and apatite fission track thermochronology, *in* Hendrix, M.S., and Davis, G.A., eds., Paleozoic and Mesozoic Tectonic Evolution of Central and Eastern Asia: From Continental Assembly to Intracontinental Deformation: Geological Society of America Memoir 194, p. 247–267, doi:10.1130/0-8137-1194-0.247.

Sobel, E.R., Hilley, G.E., and Strecker, M.R., 2003, Formation of internally drained contractional basins by aridity-limited bedrock incision: Journal of Geophysical Research–Solid Earth, v. 108, no. B7, p. 2344, doi:10.1029/2002JB001883.

Song, B., Zhang, K., Chen, R., Wang, C., Luo, M., Zhang, J., and Jiang, S., 2013a, The sedimentary record in northern Qaidam Basin and its response to the uplift of the southern Qilian Mountain at around 30 Ma: Acta Geologica Sinica, v. 87, p. 528–539, doi:10.1111/1755-6724.12066 [English edition].

Song, B., Zhang, K., Lu, J., Wang, C., and Xu, Y., 2013b, The middle Eocene to early Miocene integrated sedimentary record in the Qaidam Basin and its implications for paleoclimate and early Tibetan Plateau uplift: Canadian Journal of Earth Sciences, v. 50, p. 183–196, doi:10.1139/cjes-2012-0048.

Spurlin, M.S., Yin, A., Horton, B.K., Zhou, J., and Wang, J., 2005, Structural evolution of the Yushu-Nangqian region and its relationship to syncollisional igneous activity east-central Tibet: Geological Society of America Bulletin, v. 117, p. 1293–1317, doi:10.1130/B25572.1.

Staisch, L.M., Niemi, N.A., Hong, C., Clark, M.K., Rowley, D.B., and Currie, B., 2014, A Cretaceous–Eocene depositional age for the Fenghuoshan Group, Hoh Xil Basin: Implications for the tectonic evolution of the northern Tibet Plateau: Tectonics, v. 33, p. 281–301, doi:10.1002/2013TC003367.

Strecker, M.R., Alonso, R.N., Bookhagen, B., Carrapa, B., Hilley, G.E., Sobel, E.R., and Trauth, M.H., 2007, Tectonics and climate of the southern central Andes: Annual Review of Earth and Planetary Sciences, v. 35, p. 747–787, doi:10.1146/annurev.earth.35.031306.140158.

Sun, Z., Yang, Z., Pei, J., Ge, X., Wang, X., Yang, T., Li, W., and Yuan, S., 2005, Magnetostratigraphy of Paleogene sediments from northern Qaidam Basin, China: Implications for tectonic uplift and block rotation in northern Tibetan Plateau: Earth and Planetary Science Letters, v. 237, p. 635–646, doi:10.1016/j.epsl.2005.07.007.

Tapponnier, P., Zhiqin, X., Meyer, B., and Arnaud, N., 2001, Oblique stepwise rise and growth of the Tibet Plateau: Science, v. 294, no. 1671, p. 1671–1677, doi:10.1126/science.105978.

Taylor, M.H., Kapp, P.A., and Horton, B.K., 2012, Basin response to active extension and strike-slip deformation in the hinterland of the Tibetan Plateau, *in* Busby, C., and Azor, A., eds., Tectonics of Sedimentary Basins: Recent Advances: Oxford, UK, Blackwell Publishing Ltd., p. 445–460, doi:10.1002/9781444347166.ch22.

Tornqvist, T., 1993, Holocene alternation of meandering and anastomosing fluvial systems in the Rhine-Meuse delta (central Netherlands) controlled by sea-level rise and subsoil erodibility: Journal of Sedimentary Petrology, v. 63, p. 683–693.

Van der Woerd, J., Ryerson, F.J., Tapponnier, P., Gaudemer, Y., Finkel, R., Meriaux, A.S., and Caffee, M., 1998, Holocene left-slip rate determined by cosmogenic surface dating on the Xidatan segment of the Kunlun fault (Qinghai, China): Geology, v. 26, p. 695–698, doi:10.1130/0091-7613(1998)026<0695:HLSRDB>2.3.CO;2.

Vermeesch, P., 2012, On the visualisation of detrital age distributions: Chemical Geology, v. 312–313, p. 190–194, doi:10.1016/j.chemgeo.2012.04.021.

Vermeesch, P., 2013, Multi-sample comparison of detrital age distributions: Chemical Geology, v. 341, p. 140–146, doi:10.1016/j.chemgeo.2013.01.010.

Wang, E., Xu, F.-Y., Zhou, J.-X., Wan, J., and Burchfiel, B.C., 2006, Eastward migration of the Qaidam Basin and its implications for Cenozoic evolution of the Altyn Tagh fault and associated river systems: Geological Society of America Bulletin, v. 118, p. 349–365, doi:10.1130/B25778.1.

Wang, F., Lo, C.-H., Li, Q., Yeh, M.-W., Wan, J., Zheng, D., and Wang, E., 2004, Onset timing of significant unroofing around Qaidam Basin, northern Tibet, China: Constraints from $^{40}Ar/^{39}Ar$ and FT thermochronology on granitoids: Journal of Asian Earth Sciences, v. 24, p. 59–69, doi:10.1016/j.jseaes.2003.07.004.

Wang, Q., and Coward, M.P., 1990, The Chaidam Basin (NW China): Formation and hydrocarbon potential: Journal of Petroleum Geology, v. 13, p. 93–112, doi:10.1306/BF9AB6C2-0EB6-11D7-8643000102C1865D.

Wang, X., Qiu, Z., Li, Q., Wang, B., Qiu, Z., Downs, W.R., Xie, G., Xie, J., Deng, T., Takeuchi, G.T., Tseng, Z.J., Chang, M., Liu, J., Wang, Y., Biasatti, D., Sun, Z., Fang, X., Meng, Q., 2007,, Vertebrate paleontology, biostratigraphy, geochronology, and paleoenvironment of Qaidam Basin in northern Tibetan Plateau: Palaeogeography, Palaeoclimatology, Palaeoecology, v. 254, p. 363–385, doi:10.1016/j.palaeo.2007.06.007.

Wang, Y., Zhang, X.M., Wang, E., Zhang, A.F., Li, Q., and Sun, G.H., 2005, Ar-40/Ar-39 thermochronological evidence for formation and Mesozoic evolution of the northern-central segment of the Altyn Tagh fault system in the northern Tibetan Plateau: Geological Society of America Bulletin, v. 117, p. 1336–1346, doi:10.1130/B25685.1.

Weislogel, A.L., 2008, Tectonostratigraphic and geochronologic constraints on evolution of the northeast Paleotethys from the Songpan-Ganzi complex, central China: Tectonophysics, v. 451, p. 331–345, doi:10.1016/j.tecto.2007.11.053.

Weislogel, A.L., Graham, S.A., Chang, E.Z., Wooden, J.L., Gehrels, G.E., and Yang, H., 2006, Detrital zircon provenance of the Late Triassic Songpan-Ganzi complex: Sedimentary record of collision of the North and South China blocks: Geology, v. 34, p. 97, doi:10.1130/G21929.1.

Weislogel, A.L., Graham, S.A., Chang, E.Z., Wooden, J.L., and Gehrels, G.E., 2010, Detrital zircon provenance from three turbidite depocenters of the Middle-Upper Triassic Songpan-Ganzi complex, central China: Record of collisional tectonics, erosional exhumation, and sediment production: Geological Society of America Bulletin, v. 122, p. 2041–2062, doi:10.1130/B26606.1.

Woodruff, W.H., Horton, B.K., Kapp, P.A., and Stockli, D.F., 2013, Late Cenozoic evolution of the Lunggar extensional basin, Tibet: Implications for basin growth and exhumation in hinterland plateaus: Geological Society of America Bulletin, v. 125, p. 343–358, doi:10.1130/B30664.1.

Wu, C., Yang, J., Wooden, J.L., Shi, R., Chen, S., Meibom, A., and Mattinson, C., 2004, Zircon U-Pb SHRIMP dating of the Yematan batholith in Dulan, North Qaidam, NW China: Chinese Science Bulletin, v. 49, p. 1736–1740, doi:10.1007/BF03184308.

Xia, W., Zhang, N., Yuan, X., Fan, L., and Zhang, B., 2001, Cenozoic Qaidam Basin, China: A stronger tectonic inversed, extensional rifted basin: American Association of Petroleum Geologists Bulletin, v. 85, p. 715–736.

Xiao, W.J., Windley, B.F., Chen, H.L., Zhang, G.C., and Li, J.L., 2002, Carboniferous–Triassic subduction and accretion in the western Kunlun, China: Implications for the collisional and accretionary tectonics of the northern Tibetan Plateau: Geology, v. 30, p. 295, doi:10.1130/0091-7613(2002)030<0295:CTSAAI>2.0.CO;2.

Xiao, W., Windley, B.F., Yong, Y., Yan, Z., Yuan, C., Liu, C., and Li, J., 2009, Early Paleozoic to Devonian multiple-accretionary model for the Qilian Shan, NW China: Journal of Asian Earth Sciences, v. 35, p. 323–333, doi:10.1016/j.jseaes.2008.10.001.

Xu, Z., 1984, Tertiary System and its Petroleum Potential in the Lunpola Basin, Xizang (Tibet): Reston, U.S. Geological Survey Open-File Report 84-420, 5 p.

Yan, Z., Xiao, W.J., Windley, B.F., Wang, Z.Q., and Li, J.L., 2010, Silurian clastic sediments in the North Qilian Shan, NW China: Chemical and isotopic constraints on their forearc provenance with implications for the Paleozoic evolution of the Tibetan Plateau: Sedimentary Geology, v. 231, p. 98–114, doi:10.1016/j.sedgeo.2010.09.001.

Yang, F., Ma, Z., Xu, T., and Ye, S., 1992, A Tertiary paleomagnetic stratigraphic profile in Qaidam Basin: Acta Petrolei Sinica, v. 13, p. 97–101, doi:10.7623/syxb199202016.

Yang, J., Xu, Z., Zhang, J., Chu, C.-Y., Zhang, R., and Liou, J.-G., 2001, Tectonic significance of early Paleozoic high-pressure rocks in Altun-Qaidam-Qilian Mountains, northwest China, *in* Hendrix, M.S., and Davis, G.A., eds., Paleozoic and Mesozoic Tectonic Evolution of

Central and Eastern Asia: From Continental Assembly to Intracontinental Deformation: Geological Society of America Memoir 194, p. 151–170, doi:10.1130/0-8137-1194-0.151.

Yang, Y., Ritzwoller, M.H., Zheng, Y., Shen, W., Levshin, A.L., and Xie, Z., 2012, A synoptic view of the distribution and connectivity of the mid-crustal low velocity zone beneath Tibet: Journal of Geophysical Research–Solid Earth (1978–2012), v. 117, p. B04303, doi:10.1029/2011JB008810.

Yin, A., and Harrison, T.M., 2000, Geologic evolution of the Himalayan-Tibetan orogen: Annual Review of Earth and Planetary Sciences, v. 28, no. 1, p. 211–280, doi:10.1146/annurev.earth.28.1.211.

Yin, A., Butler, R., Harrison, T.M., Foster, D.A., Ingersoll, R.V., Zhou, X., Wang, X.-F., and Hanson, A.D., 2002, Tectonic history of the Altyn Tagh fault system in northern Tibet inferred from Cenozoic sedimentation: Geological Society of America Bulletin, v. 114, p. 1257–1295, doi:10.1130/0016-7606(2002)114<1257:THOTAT>2.0.CO;2.

Yin, A., Dang, Y.-Q., Zhang, M., McRivette, M.W., Burgess, W.P., and Chen, X.-H., 2007a, Cenozoic tectonic evolution of Qaidam Basin and its surrounding regions (part 2): Wedge tectonics in southern Qaidam Basin and the Eastern Kunlun Range, *in* Sears, J.W., Harms, T.A., and Evenchick, C.A., eds., Whence the Mountains? Inquiries into the Evolution of Orogenic Systems: A Volume in Honor of Raymond A. Price: Geological Society of America Special Paper 433, p. 369–390, doi:10.1130/2007.2433(18).

Yin, A., Manning, C.E., Lovera, O., Menold, C.A., Chen, X., and Gehrels, G.E., 2007b, Early Paleozoic tectonic and thermomechanical evolution of ultrahigh-pressure (UHP) metamorphic rocks in the northern Tibetan Plateau, Northwest China: International Geology Review, v. 49, p. 681–716, doi:10.2747/0020-6814.49.8.681.

Yin, A., Dang, Y.-Q., Wang, L.-C., Jiang, W.-M., Zhou, S.-P., Chen, X.-H., Gehrels, G.E., and McRivette, M.W., 2008a, Cenozoic tectonic evolution of Qaidam Basin and its surrounding regions (Part 1): The southern Qilian Shan–Nan Shan thrust belt and northern Qaidam Basin: Geological Society of America Bulletin, v. 120, p. 813–846, doi:10.1130/B26180.1.

Yin, A., Dang, Y.-Q., Zhang, M., Chen, X.-H., and McRivette, M.W., 2008b, Cenozoic tectonic evolution of the Qaidam Basin and its surrounding regions (Part 3): Structural geology, sedimentation, and regional tectonic reconstruction: Geological Society of America Bulletin, v. 120, p. 847–876, doi:10.1130/B26232.1.

Yuan, C., Sun, M., Xiao, W., Wilde, S., Li, X., Liu, X., Long, X., Xia, X., Ye, K., and Li, J., 2009, Garnet-bearing tonalitic porphyry from East Kunlun, northeast Tibetan Plateau: Implications for adakite and magmas from the MASH zone: International Journal of Earth Sciences, v. 98, p. 1489–1510, doi:10.1007/s00531-008-0335-y.

Yuan, D.-Y., Ge, W.-P., Chen, Z.-W., Li, C.-Y., Wang, Z.-C., Zhang, H.-P., Zhang, P.-Z., Zheng, D.-W., Zheng, W.-J., Craddock, W.H., Dayem, K.E., Duvall, A.R., Hough, B.G., Lease, R.O., Champagnac, J.-D., Burbank, D.W., Clark, M.K., Farley, K.A., Garzione, C.N., Kirby, E., Molnar, P., and Roe, G.H., 2013, The growth of northeastern Tibet and its relevance to large-scale continental geodynamics: A review of recent studies: Tectonics, v. 32, p. 1358–1370, doi:10.1002/tect.20081.

Yuan, W., Dong, J., Shicheng, W., and Carter, A., 2006, Apatite fission track evidence for Neogene uplift in the eastern Kunlun Mountains, northern Qinghai–Tibet Plateau, China: Journal of Asian Earth Sciences, v. 27, p. 847–856, doi:10.1016/j.jseaes.2005.09.002.

Yue, Y., Ritts, B.D., Graham, S.A., Wooden, J.L., Gehrels, G.E., and Zhang, Z., 2004, Slowing extrusion tectonics: Lowered estimate of post–Early Miocene slip rate for the Altyn Tagh fault: Earth and Planetary Science Letters, v. 217, p. 111–122, doi:10.1016/S0012-821X(03)00544-2.

Yue, Y., Graham, S.A., Ritts, B.D., and Wooden, J.L., 2005, Detrital zircon provenance evidence for large-scale extrusion along the Altyn Tagh fault: Tectonophysics, v. 406, p. 165–178, doi:10.1016/j.tecto.2005.05.023.

Zahid, K.M., and Barbeau, D.L., 2011, Constructing sandstone provenance and classification ternary diagrams using an electronic spreadsheet: Journal of Sedimentary Research, v. 81, p. 702–707, doi:10.2110/jsr.2011.55.

Zhang, C.L., Lu, S.N., Yu, H.F., and Ye, H.M., 2007, Tectonic evolution of the Western Kunlun orogenic belt in northern Qinghai-Tibet Plateau: Evidence from zircon SHRIMP and LA-ICP-MS U-Pb geochronology: Science in China, ser. D, Earth Science, v. 50, p. 825–835, doi:10.1007/s11430-007-2051-z.

Zhang, H.-P., Craddock, W.H., Lease, R.O., Wang, W., Yuan, D.-Y., Zhang, P.-Z., Molnar, P., Zheng, D.-W., and Zheng, W.-J., 2012, Magnetostratigraphy of the Neogene Chaka basin and its implications for mountain building processes in the north-eastern Tibetan Plateau: Basin Research, v. 24, p. 31–50, doi:10.1111/j.1365-2117.2011.00512.x.

Zhang, J.Y., Ma, C.Q., Xiong, F.H., and Liu, B., 2012, Petrogenesis and tectonic significance of the Late Permian–Middle Triassic calc-alkaline granites in the Balong region, eastern Kunlun orogen, China: Geological Magazine, v. 149, p. 892–908, doi:10.1017/S0016756811001142.

Zhang, P.Z., Shen, Z., Wang, M., Gan, W., Bürgmann, R., Molnar, P., Wang, Q., Niu, Z., Sun, J., Wu, J., Hanrong, S., and Xinzhao, Y., 2004, Continuous deformation of the Tibetan Plateau from global positioning system data: Geology, v. 32, p. 809–812, doi:10.1130/G20554.1.

Zhang, W.L., 2006, Cenozoic uplift of the Tibetan Plateau: evidence from high resolution magnetostratigraphy of the Qaidam basin: Lanzhou University, 245 p.

Zhang, Y., and Zheng, J., 1994, Geologic Overview in Kokshili, Qinghai and Adjacent Areas: Beijing, Seismological Publishing House, 177 p.

Zheng, D., Clark, M.K., Zhang, P., Zheng, W., and Farley, K.A., 2010, Erosion, fault initiation and topographic growth of the North Qilian Shan (northern Tibetan Plateau): Geosphere, v. 6, p. 937–941, doi:10.1130/GES00523.1.

Zhuang, G., Hourigan, J.K., Ritts, B.D., and Kent-Corson, M.L., 2011, Cenozoic multiple-phase tectonic evolution of the northern Tibetan Plateau: Constraints from sedimentary records from Qaidam Basin, Hexi Corridor, and Subei Basin, northwest China: American Journal of Science, v. 311, p. 116–152, doi:10.2475/02.2011.02.

MANUSCRIPT RECEIVED 19 FEBRUARY 2015
REVISED MANUSCRIPT RECEIVED 15 OCTOBER 2015
MANUSCRIPT ACCEPTED 4 NOVEMBER 2015

Printed in the USA